



# Mass transport induced by infragravity waves

Zhiling Liao<sup>1</sup>  and Qingping Zou<sup>1</sup> 

<sup>1</sup>The Lyell Centre for Earth and Marine Science and Technology, Institute for Infrastructure and Environment, Heriot-Watt University, Edinburgh EH14 4AS, UK

**Corresponding author:** Qingping Zou, [q.zou@hw.ac.uk](mailto:q.zou@hw.ac.uk)

(Received 9 September 2024; revised 31 March 2025; accepted 28 May 2025)

Mass transport induced by group-forced subharmonic waves (infragravity waves) is investigated in the present study. A theoretical solution for subharmonic waves' kinematic contributions to fourth-order mass transport and drift velocity has been proposed for any depth and bandwidth for the first time. This model is validated using particle-tracking simulations driven by the flow field generated by the SWASH. The subharmonic-induced mass transport solution is a weighted sum of the subharmonic velocity variance spectrum and velocity skewness bispectrum due to the triad-difference interaction among two primary and one subharmonic components. For narrow-banded waves with long wave group relative to depth, the weightings become independent of spectral components, and the solution is recovered in the time domain. Two mechanisms contributing to mass transport were identified: a forward drift resulting from self-interaction similar to Stokes drift, and a depth-decaying backward drift induced by negative subharmonic velocity skewness due to the anti-phase coupling between subharmonics and wave groups. For narrow-banded waves the forward transport surpasses the backward transport for  $kh < 0.72$ , where  $k$  is the short wave wavenumber and  $h$  is the water depth. For other waves, the critical  $kh$  for this phenomenon decreases with increasing wave period and bed slope and decreasing bandwidth. At greater depths or steeper bed slopes, near-surface backward transport predominates over forward transport; at shallower depths or gentler slopes, forward transport is dominant throughout the water column. Although smaller than Stokes transport by short waves, the subharmonic wave-induced mass transport can affect the long-term trajectory of a floating and suspended particle. This study provides the first evidence and insight for the influences of group-forced subharmonics on vertically varying mass transport from the ocean surface to seabed in coastal environments.

**Key words:** surface gravity waves, sediment transport, coastal engineering

## 1. Introduction

Mass transport by waves has been widely studied due to its crucial role in transporting material in the ocean, such as coastal sediment (Henderson & Allen 2004; Hsu, Elgar & Guza 2006; Ruessink *et al.* 2011; Miles 2013; Li *et al.* 2024), spilt oil (Christensen & Terrile 2009; Drivdal, Broström & Christensen 2014; Laxague *et al.* 2018) and marine plastics (DiBenedetto *et al.* 2018, 2022; Calvert *et al.* 2019, 2021; van Sebille *et al.* 2020; Núñez *et al.* 2023; Liao *et al.* 2024).

For non-breaking waves, mass transport occurs due to both the rotational wave motion near the surface and bottom boundary layers and the irrotational motion in the core region outside the boundary layers (Longuet-Higgins 1953). Inside the boundary layer the horizontal and vertical velocities are no longer in quadrature, their correlation gives rise to wave radiation stress which generates a Eulerian steady streaming inside the near-bed wave boundary layer and a steady vorticity in the free-surface boundary layer (Russell & Osorio 1957; Longuet-Higgins 1960; Zou 2002; Zou & Hay 2003; Zou, Bowen & Hay 2006). Both the steady streaming and the steady vorticity outside the boundary layer drive the mass transport in the core fluid region (Iskandarani & Liu 1991; Vittori & Blondeaux 1996; Blondeaux, Brocchini & Vittori 2002; Ng 2004*a,b*).

Fluid particles in the irrotational core region experience a net forward drift known as the Stokes drift due to the non-closed trajectory over each wave cycle (Stokes 1847). For a monochromatic progressive wave with amplitude  $a$ , angular frequency  $\omega$  and wavenumber  $k$  at constant depth  $h$ , the first-order surface elevation and velocity field are given by  $\eta = a \cos(kx - \omega t)$  and

$$\begin{cases} u = a\omega \frac{\cosh[k(z+h)]}{\sinh kh} \cos(kx - \omega t), \\ w = a\omega \frac{\sinh[k(z+h)]}{\sinh kh} \sin(kx - \omega t), \end{cases} \quad (1.1)$$

where  $z$  is positive upward with  $z = 0$  at the still water level. The first-order trajectory of a particle can thus be obtained by integrating (1.1) with time as illustrated in figure 1. The Stokes drift velocity can be derived from the net drift after a wave cycle (Ursell 1953)

$$U_s = \overline{\int u dt \frac{\partial u}{\partial x} + \int w dt \frac{\partial u}{\partial z}} = \frac{(ak)^2 c}{2} \frac{\cosh[2k(z+h)]}{\sinh^2 kh}, \quad (1.2)$$

where  $c = \omega/k$  is the wave propagation speed. Integrating  $\rho U_s$  across the water column yields the Stokes transport

$$\int_{-h}^0 \rho U_s dz = \frac{\rho g a^2}{2c} = \frac{E}{c} \quad (1.3)$$

where  $E = \rho g a^2/2$  is the wave energy,  $\rho$  is the fluid density,  $g$  is the gravitational acceleration.

Besides examining the trajectory of a Lagrangian particle, Stokes transport can also be obtained in an Eulerian system. In the first-order problem, the velocity in (1.1) is always defined from the bottom  $z = -h$  up to  $z = 0$  even during  $\eta < 0$  when physically there is no velocity between  $z = \eta$  and  $z = 0$ . The velocity in the wave trough area given by (1.1) is therefore virtual and represents the analytical extension of the actual velocity from  $z = \eta$  to  $z = 0$  and, by the same argument, from  $z = 0$  to  $z = \eta$  in the crest area during  $\eta > 0$ . Effectively, the wave crest where  $\eta > 0$  carries ‘positive’ mass forward while the wave trough where  $\eta < 0$  carries ‘negative’ mass backward (Longuet-Higgins 1969). Therefore, the residual

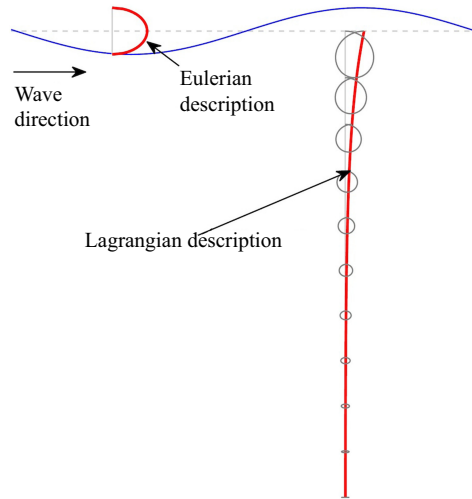


Figure 1. Schematic of the Eulerian and Lagrangian descriptions of mass transport induced by a progressive wave.

net forward mass transport is approximately  $\overline{\rho u|_{z=0}\eta}$ , which leads to the same result of  $E/c$ . Physically, the horizontal velocity observed by a sensor at a fixed height  $z = z_o$  between wave crest and trough ( $-a \leq z_o \leq a$ ) is intermittently zero when  $z_o > \eta$  as

$$u|_{z=z_o} = \begin{cases} a\omega \frac{\cosh[k(z_o + h)]}{\sinh kh} \cos(kx - \omega t) & z_o \leq \eta, \\ 0 & z_o > \eta, \end{cases} \quad (1.4)$$

which yields a non-zero forward mean velocity  $\bar{u}(z_o)$  between the crest and trough, as illustrated in figure 1, and hence a forward net mass transport equal to  $\int_{-a}^a \rho \bar{u} dz_o$ . The first-order particle orbits and thus mass transport can be significantly modified by higher-order nonlinear harmonics. Using a perturbation method, Chen, Hsu & Chen (2010) derived the Lagrangian solution of particle trajectory for monochromatic progressive waves over a flat bottom up to fifth order. Chen *et al.* (2012) extended the flat bottom solution to a sloping bottom case up to third order. Recently, Li *et al.* (2023) obtained the particle trajectory solution for partial reflected waves over a sloping bottom. However, these studies adopted monochromatic waves as the leading-order wave, therefore, do not account for the effect of second-order subharmonic waves generated through difference interaction between first-order waves (primary waves) of different frequencies. As a result, subharmonic wave-induced mass transport has not been studied to authors' knowledge.

The subharmonic wave is often regarded as an infragravity wave as its period falls into the infragravity band of 25~250 s (Bertin *et al.* 2018). They are generated by energy transfer from short waves propagating into nearshore shallow water (Norheim, Herbers & Elgar 1998; Sheremet *et al.* 2002; de Bakker *et al.* 2015) driven by the wave group-modulated radiation stress gradient. When short waves break in the surf zone, infragravity wave height may grow up to over 1 m towards the shore from a few centimetres in the offshore. For example, the well-known surf beats observed by Munk (1949) and Tucker (1950) are one kind of infragravity wave in the surf zone. Infragravity waves are related to various nearshore and coastal processes such as rip currents, run-up/overtopping, as well as beach and dune erosion (Russell 1993; de Vries *et al.* 2008; Castle *et al.* 2016; Bertin *et al.* 2018). When the depth is shallow relative to the wave group length but not the short wavelength, explicit theoretical solutions of the group-forced subharmonic were obtained

for a flat bottom (Longuet-Higgins & Stewart 1962; Davey & Stewartson 1974; Mei *et al.* 2005) and a slowly varying bathymetry (Janssen, Battjes & van Dongeren 2003; Zou 2011). Calvert *et al.* (2019) recently extended the solution to arbitrary depth relative to the wave group length. However, those solutions diverge when the subharmonic response to wave group forcing approaches resonance as the depth becomes shallow relative to the short wavelength. In this case, solutions in integral form were derived for a plane sloping bed (Symonds, Huntley & Bowen 1982; van Leeuwen 1992; Schäffer 1993) and for a slowly varying bathymetry (Liao *et al.* 2021, 2023).

However, despite improved understanding of generation and evolution of subharmonic waves in the past years, not until recently did its effect on particle movements start to be recognised. The low-frequency infragravity wave motion causes large excursion of water particles because the particle excursion is proportional to wave period (Bondehagen, Kalisch & Roeber 2024). Calvert *et al.* (2019) showed how the set down in a transient wave group affects the particle drift throughout the water column. Bjørnstad *et al.*'s (2021) Lagrangian measurements in the surf zone indicate that infragravity waves may trigger short wave breaking by enhancing the peak forward particle velocity at the surface. Through theory and field observations, Herbers & Janssen (2016) observed energetic infragravity fluctuations in the drift velocity of surface buoy in deep water that are several orders of magnitude larger and out of phase with the Eulerian infragravity motions. McAllister & van den Bremer (2019) found the Lagrangian measurement of surface drifter is significant in the group-bounded subharmonic band, which affects the 'apparent' steepness derived from time histories of drifter motion and poses a potential issue for wave buoys to measure acceleration. Flores, Williams & Horner-Devine (2022) show the first measurements of infragravity waves' modulation of salinity near a river plume.

Although little is known about subharmonic wave-induced mass transport, the contribution of subharmonic waves to sediment transport are well recognised. In intermediate water, group-forced subharmonics are in anti-phase coupling with short wave groups, therefore, backward transport of high concentration sediment under large waves and subharmonic wave troughs exceeds forward transport of low concentration sediment under small waves and subharmonic wave crests, leading to net backwards sediment transport. As waves shoal and break in the nearshore, the phase relationship between subharmonic wave and wave groups evolves, which in turn alters the net sediment transport by group-forced subharmonic (Deigaard, Jakobsen & Fredsøe 1999; Baldock *et al.* 2010, 2011; de Bakker *et al.* 2016a). On some occasions, infragravity waves may contribute to up to 60 % of onshore transport of suspended sediment in the inner surf zone over a gently sloping beach (de Bakker *et al.* 2016a). Besides the sediment transport due to coupling between short waves and infragravity waves, field measurements indicated that onshore sediment transport may be induced by tidal-modulated infragravity waves in wave-dominated inlets or shallow and small estuaries (Bertin & Olabarrieta 2016; Williams & Stacey 2016; Bertin *et al.* 2019; Mendes *et al.* 2020).

Currently, the literature on subharmonic wave-induced mass transport is scarce. In this work, theoretical solutions of the mass transport and the associated drift velocity induced by group-forced subharmonic waves in the shoaling zone are derived for the first time. The model is validated by the GLOBEX experiment (Ruessink *et al.* 2013). It was also validated against the mass transport velocity obtained by Lagrangian particle-tracking simulations using the flow field generated by the non-hydrostatic wave model SWASH (Zijlema, Stelling & Smit 2011). The theoretical solutions reveal two distinct kinematic mechanisms for subharmonic wave-induced mass transport: the forward transport in analogy to the Stokes transport of short waves, and the backward transport due to the anti-phase coupling between subharmonic waves and wave groups. The latter is proportional

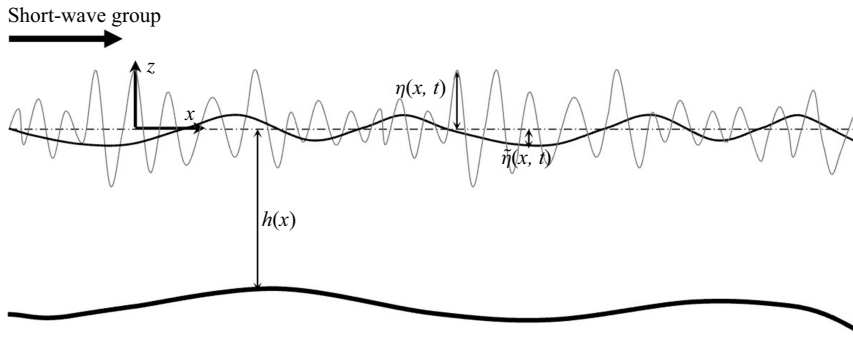


Figure 2. Definition sketch of variables and coordinate system for a short wave group propagating over an undulating bottom topography with mild slope. Here,  $\eta$  and  $\tilde{\eta}$  denote total surface elevation and the second-order subharmonic wave underneath the short wave group.

to the velocity skewness contributed by subharmonic waves. The theoretical model is combined with the SWASH model and the GLOBEX experiment (Ruessink *et al.* 2013) to examine the role of water depth, bed slope, wave period and bandwidth. The newly proposed subharmonic wave-induced mass transport provides the third mechanism for sediment transport in addition to the well-known boundary layer streaming (Nielsen 2006) and suspension-advection mechanisms (Deigaard *et al.* 1999). The subharmonic wave-induced mass transport is distributed throughout the water column hence is also expected to affect the transport of buoyant particles such as microplastics.

The paper is organised as follows. The theoretical solution of subharmonic wave surface elevation and velocity as well as the subharmonic wave-induced mass transport velocity and the bulk transport are derived and compared with the GLOBEX experiment in § 2. The set-up and postprocessing of the SWASH model and the Lagrangian particle-tracking simulation are described in § 3.1. Results of simulated particle trajectory, mass transport velocity and mass transport are demonstrated and compared with theoretical solutions in § 3.2. Discussions and conclusions are provided in § 4.

## 2. Theory of subharmonic wave-induced mass transport

### 2.1. Surface elevation and horizontal velocity of subharmonic wave

Consider shoaling unidirectional irregular waves propagating in the positive  $x$ -direction over an undulating seabed described by  $z = -h(x)$ . Let  $z = \eta(x, t)$  and  $u(x, z, t)$  be the surface elevation and horizontal velocity of the waves, respectively. The small parameter corresponding to amplitude is denoted by short wave steepness  $\varepsilon \equiv ka$ , where  $a$  and  $k$  are the characteristic wave amplitude and wavelength, respectively. The asymptotic expansion of  $\eta$  and  $u$  is given by

$$\left. \begin{aligned} u &= u^{(1)} + u^{(2)} + \dots \\ \eta &= \eta^{(1)} + \eta^{(2)} + \dots \end{aligned} \right\}, \quad (2.1)$$

where the superscript  $(i)$  denotes the variables at the order of  $O(\varepsilon^i)$ .

Assume  $\eta^{(1)}$  has frequency band  $[\omega_p(1 - \alpha), \omega_p(1 + \alpha)]$  and can be written in the form of a discrete Fourier series

$$\left\{ \begin{aligned} \eta^{(1)}(x, t) &= \text{Re} \left[ \sum_{n=n_1}^{n_1+N} \hat{a}_n(x) \exp i\theta_n \right], \\ \theta_n &= \int_{x_0}^x k_n dx' - \omega_n t, \end{aligned} \right. \quad (2.2)$$

where  $\omega_n = n\Delta\omega$  is the radian frequency ( $\Delta\omega$  = frequency resolution) for the  $n$ th component,  $k_n$  is the wavenumber satisfying the dispersion relationship  $\omega_n^2 = gk_n \tanh k_n h$ ,  $\hat{a}_n$  is the complex amplitude,  $n_1$  is the index of the lower limit frequency  $N$  is the number of frequency components and  $Re[\cdot]$  denotes the real part of the complex argument and will be omitted herein after for brevity.

Letting  $h_x \equiv dh/dx$  and  $h_{xx} \equiv d^2h/dx^2$ , we make following assumptions on the parameters:

$$\varepsilon \ll (kh)^3, \quad \alpha = O(\varepsilon), \quad \varepsilon kh \ll 1, \quad |h_x| = O(\varepsilon^n kh) \quad (n > 1), \quad |h_{xx}| = O(\varepsilon^{2n} k^2 h), \quad (2.3)$$

which is equivalent to the assumptions in Zou (2011).

Accordingly, the first-order horizontal velocity is given by

$$\left\{ \begin{aligned} u^{(1)}(x, z, t) &= \sum_{n=n_1}^{n_1+N} \hat{u}_n(x) \frac{\cosh[k_n(z+h)]}{\cosh k_n h} \exp i\theta_n, \\ \hat{u}_n(x) &= \frac{\hat{a}_n(x)\omega_n}{\tanh k_n h}. \end{aligned} \right. \quad (2.4)$$

Assuming the complex amplitude  $\hat{a}_n(x)$  only changes in magnitude following the conservative shoaling

$$\frac{\hat{a}_n(x)}{\hat{a}_n(x_0)} = \sqrt{\frac{c_g(x_0)}{c_g(x)}}, \quad c_g = \left. \frac{\partial \omega}{\partial k} \right|_{\omega=\omega_p} = \sqrt{\frac{g \tanh k_p h}{k_p}} \left( \frac{1}{2} + \frac{k_p h}{\sinh 2k_p h} \right), \quad (2.5)$$

where  $c_g$  is the wave group speed corresponding to central frequency  $\omega_p$ , and (2.2) can be rewritten as

$$\eta^{(1)}(x, t) = A(x, t) \exp \left[ i \left( \int_{x_0}^x k_p dx' - \omega_p t \right) \right], \quad (2.6)$$

where the modulated complex amplitude  $A(x, t)$  is given by

$$\left\{ \begin{aligned} A(x, t) &= \sum_{n=n_1}^{n_1+N} \hat{a}_n(x) \exp \left[ i \left( \int_{x_0}^x k_{n,p} dx' - \omega_{n,p} t \right) \right], \\ \omega_{n,p} &= \omega_p - \omega_n, \quad k_{n,p} = k_n - k_p. \end{aligned} \right. \quad (2.7)$$

Substituting (2.7) into the formula for wave energy  $E = \rho g |A|^2/2$  yields the modulated wave energy

$$\left\{ \begin{aligned} E(x, t) &= \bar{E}(x) + \tilde{E}(x, t) \\ \bar{E}(x) &= \frac{1}{2} \rho g \sum_{n=n_1}^{n_1+N} |\hat{a}_n(x)|^2, \\ \tilde{E}(x, t) &= \rho g \sum_{m=n_1}^{n_1+N} \sum_{n=n_1}^{m-1} \hat{a}_m(x) \hat{a}_n^*(x) \exp \left[ i \left( \int_{x_0}^x k_{m,n} dx' - \omega_{m,n} t \right) \right], \\ \omega_{m,n} &= \omega_m - \omega_n, \quad k_{m,n} = k_m - k_n, \end{aligned} \right. \quad (2.8)$$

where  $\bar{E}$  and  $\tilde{E}$  denote the steady and unsteady components of the wave energy, respectively,  $n_1$  is the index of the lower limit frequency of  $\eta^{(1)}$  and  $N$  is the number of frequency components of  $\eta^{(1)}$ . The density  $\rho$  is omitted hereinafter for being constant and for brevity. Throughout this paper  $\widetilde{(\cdot)}$  and  $\overline{(\cdot)}$  denote the low-frequency unsteady and steady components of a time-dependent variable, which are equivalent to averaging over the short wave and wave group phase, respectively.

Since  $\omega_{m,n} = \omega_m - \omega_n = \omega_{m-n}$ ,  $\tilde{E}(x, t)$  in (2.8) can be rewritten by letting  $m - n \rightarrow l$  and  $\omega_{m,n} \rightarrow \omega_l$  and changing one of the double summations into the sum over new index  $l$

$$\begin{aligned}\tilde{E}(x, t) &= g \sum_{l=1}^N \sum_{m=n_1}^{n_1+N} \hat{a}_m(x) \hat{a}_{m-l}^*(x) \exp \left[ i \left( \int_{x_0}^x k_{m,m-l} dx' - \omega_l t \right) \right] \\ &= g \sum_{l=1}^N \left[ \sum_{m=n_1}^{n_1+N} \hat{a}_m(x) \hat{a}_{m-l}^*(x) \right] \exp \left[ i \left( \int_{x_0}^x k_l dx' - \omega_l t \right) + O(\varepsilon) \right],\end{aligned}\quad (2.9)$$

where

$$\omega_l = O(\varepsilon \omega_p), \quad k_l = \frac{\omega_l}{c_g} = O(\varepsilon k), \quad (2.10)$$

is the radian frequency and wavenumber of the wave group. The unsteady wave energy  $\tilde{E}$  can be expressed in terms of discrete Fourier series

$$\tilde{E}(x, t) = \sum_{l=1}^N \hat{E}(x, \omega_l) \exp(-i\omega_l t), \quad (2.11)$$

and comparing (2.11) with (2.9) yields

$$\begin{cases} \hat{E}(x, \omega_l) = \hat{E}(x_0, \omega_l) \frac{c_g(x_0)}{c_g(x)} \exp \left[ i \int_{x_0}^x k_l dx' + O(\varepsilon) \right], \\ \hat{E}(x_0, \omega_l) = g \left[ \sum_{m=n_1}^N \hat{a}_m(x_0) \hat{a}_{m-l}^*(x_0) \right]. \end{cases} \quad (2.12)$$

Let  $\tilde{\eta}$ ,  $\tilde{u}$  and  $\tilde{Q}$  denote respectively the low-frequency surface elevation, horizontal velocity and volume flux, then, accurate to  $O(\varepsilon^2)$ ,  $\tilde{Q}$  can be written (Longuet-Higgins 1969; Monismith *et al.* 2007)

$$\tilde{Q} = \tilde{u}h + \frac{\tilde{E}}{c} + O(\varepsilon^4), \quad (2.13)$$

which has contributions from both the depth-uniform subharmonic orbital velocity  $\tilde{u}(x, t)$  and the modulated Stokes transport  $\tilde{E}/c$ . The linearised governing equations of  $\tilde{\eta}$  and  $\tilde{Q}$  are (Longuet-Higgins & Stewart 1962; Zou 2011; Liao *et al.* 2023)

$$\begin{cases} \frac{\partial \tilde{\eta}}{\partial t} + \frac{\partial \tilde{Q}}{\partial x} = 0, \\ \frac{\partial \tilde{Q}}{\partial t} + gh \frac{\partial \tilde{\eta}}{\partial x} = -\frac{\partial \tilde{S}}{\partial x}, \end{cases} \quad (2.14)$$

where  $\tilde{S}(x, t)$  is the modulated wave radiation stress given by (Longuet-Higgins & Stewart 1962)

$$\tilde{S} = \tilde{E} \left( \frac{2c_g}{c} - \frac{1}{2} \right). \quad (2.15)$$

Similar to (2.11), we write  $\tilde{\eta}$ ,  $\tilde{u}$ ,  $\tilde{M}$  and  $\tilde{S}$  as discrete Fourier series

$$(\tilde{\eta}, \tilde{u}, \tilde{Q}, \tilde{S}) = \sum_{l=1}^N [\hat{\eta}(x, \omega_l), \hat{u}(x, \omega_l), \hat{Q}(x, \omega_l), \hat{S}(x, \omega_l)] \exp(-i\omega_l t), \quad (2.16)$$

where the argument  $\omega_l$  for complex amplitude will be omitted hereinafter for brevity. The complex amplitude  $\hat{Q}$  and  $\hat{S}$  can be derived by substituting (2.11)–(2.12) into (2.13) and (2.15), respectively,

$$\left\{ \begin{array}{l} \hat{Q}(x) = \hat{u}h + \frac{\hat{E}}{c} \cong \hat{u}h + \frac{\hat{E}(x_0)}{c} \frac{c_g(x_0)}{c_g(x)} \exp\left(i \int_{x_0}^x k_l dx'\right), \\ \hat{S}(x) = \hat{E} \left( \frac{2c_g}{c} - \frac{1}{2} \right) \cong \left( \frac{2c_g}{c} - \frac{1}{2} \right) \hat{E}(x_0) \frac{c_g(x_0)}{c_g(x)} \exp\left(i \int_{x_0}^x k_l dx'\right). \end{array} \right. \quad (2.17)$$

Substituting (2.16) into (2.14) yields the governing equation for  $\hat{\eta}$  and  $\hat{Q}$

$$\left\{ \begin{array}{l} \hat{\eta}(x) = \frac{1}{i\omega_l} \frac{\partial \hat{Q}}{\partial x}, \\ \hat{Q}(x) = \frac{1}{i\omega_l} \frac{\partial \hat{S}}{\partial x} + \frac{gh}{i\omega_l} \frac{\partial \hat{\eta}}{\partial x}. \end{array} \right. \quad (2.18)$$

We note that the derivation from (2.1) to (2.18) essentially repeats many existing theoretical studies of the group-forced subharmonic over a mild sloping bottom (Liu 1989; van Leeuwen 1992; Schäffer 1993; Janssen *et al.* 2003; Battjes *et al.* 2004; Zou 2011; Contardo *et al.* 2021; Liao *et al.* 2021).

Over a mild bottom slope relative to the wave group length scale with the following parameter regime:

$$\beta = \frac{h_x}{k_l h} = O(\varepsilon^{n-1}) \ll 1, \quad \frac{h_{xx}}{k_l^2 h} = O(\varepsilon^{2n-2}) = O(\beta^2), \quad (2.19)$$

the solution of  $\hat{\eta}$  accurate to  $O(\beta)$  under the off-resonance condition

$$\frac{\beta}{\mu} = O(\beta), \quad \mu = 1 - \frac{c_g^2}{gh}, \quad (2.20)$$

in intermediate depth is taken from the existing literature (Janssen *et al.* 2003; Zou 2011; Liao *et al.* 2021)

$$\begin{aligned} \hat{\eta}(x) = & -\frac{\hat{S}}{gh\mu} \left\{ 1 + \frac{i\beta}{\mu} \left[ (1-\mu) \frac{d}{d \ln h} \ln \left[ \left( \frac{2c_g}{c} - \frac{1}{2} \right)^2 c_g^{-3} \right] - \frac{d}{d \ln h} \ln(h\mu^2) \right] \right. \\ & \left. + O(\beta^2) \right\}, \end{aligned} \quad (2.21)$$

where  $\hat{S}(x)$  is given in (2.17). The parameter  $\mu$  describes the extent of deviation from resonance (Janssen *et al.* 2003) and decreases from unity in deep water to zero at shallow water as  $kh \rightarrow 0$ , and  $\beta$  measures the bed slope relative to the wave group length scale (Battjes *et al.* 2004). As  $kh \rightarrow 0$ , the  $O(\beta)$  terms in (2.21) increase in magnitude as

$$\frac{\beta}{\mu} = O\left(\frac{\varepsilon^{n-1}}{(kh)^2}\right), \quad (2.22)$$

hence approaching  $O(1)$  when  $kh$  approaches  $\varepsilon^{(n-1)/2}$  (the so-called near-resonance condition). In this case, the off-resonant solution (2.21) starts to diverge and is no longer valid.

Without assuming the depth and resonance regime, Liao *et al.* (2023) obtained the leading-order solution of  $\hat{\eta}$  as ((B11) therein)

$$\left\{ \begin{aligned} \hat{\eta}(x) &= \hat{\eta}_f^+(x_0) \hat{\eta}_h^+(x, x_0) + \hat{\eta}_f^-(x_0) \hat{\eta}_h^-(x, x_0) \\ &\quad + \int_{x_0}^x \frac{k_f^2}{2ik_f gh} \hat{S} [\hat{\eta}_h^+(x, x') - \hat{\eta}_h^-(x, x')] dx', \\ \hat{\eta}_h^\pm(x_2, x_1) &= \left[ \frac{h(x_2)}{h(x_1)} \right]^{-0.25} \exp\left(i \int_{x_1}^{x_2} \pm k_f dx'\right), \end{aligned} \right. \quad (2.23)$$

with an error factor  $1 + O(\beta)$ , where  $k_f = \omega_l / \sqrt{gh}$  is the wavenumber of shallow-water waves at wave group frequency  $\omega_l$ ;  $\hat{\eta}_f^+$  and  $\hat{\eta}_f^-$  are the complex amplitudes of forward and backward propagating subharmonic waves of frequency  $\omega_l$ , respectively;  $x_0$  is the boundary for integration where  $\hat{\eta}_f^\pm(x_0)$  is known; function  $\hat{\eta}_h^\pm(x_2, x_1)$  describes the change in complex amplitude as a shallow-water wave propagates from  $x_1$  to  $x_2$ . Liao *et al.* (2023) derived (2.23) using a novel Green's function. Unlike previous solutions, the Green's function-based solution treats all subharmonic waves as free harmonics continuously radiated at shallow-water wave speed away from each point source in the forcing field of the group modulated wave radiation stress gradient, phase locked with the wave group. The solution describes the generation, propagation and interference of freely propagating subharmonic waves without distinguishing between free and bound waves. It was shown that the superposition of these free harmonics results in what are termed bound subharmonics, due to the modulation of each free harmonic's phase by the wave group. Additionally, it was demonstrated that, during shoaling, the radiated subharmonic waves propagating with the wave groups accumulate energy along the travel distance, leading to their rapid growth and the phase lag with respect to the wave groups.

It was also shown in Liao *et al.* (2023) that (2.21) can be decomposed into  $\hat{\eta} = \hat{\eta}^+ + \hat{\eta}^-$  as follows:

$$\begin{aligned} \hat{\eta}^\pm(x) &= \mp \frac{\hat{S}}{gh\mu} \frac{k_l \pm k_f}{2k_f} \left[ 1 - i\beta \frac{d}{d\ln h} \ln \left[ \left( \frac{2c_g}{c} - \frac{1}{2} \right)^2 c_g^{-3} \right] \right. \\ &\quad \left. - \beta \frac{k_l \pm k_f}{ik_l \mu} \frac{d}{d\ln h} \ln \left[ \left( \frac{2c_g}{c} - \frac{1}{2} \right) \frac{1}{c_g h^{0.25} \mu} \right] - \frac{\beta}{ik_l \mu} \frac{d}{d\ln h} (k_l \pm k_f) + O(\beta^2) \right], \end{aligned} \quad (2.24)$$

where the subscripts  $+$  and  $-$  denote the forward and backward propagating components, respectively. The parameter  $\hat{\eta}_l^\pm$  in (2.24) will be used as the boundary values  $\hat{\eta}_f^\pm(x_0)$  at  $x = x_0$  in (2.23). It follows that the model only considers the backward propagating component generated by the forcing of radiation stress gradient and thus does not account for subharmonic waves reflected from the bathymetry or the shoreline. This can be seen from the fact that the decomposition of  $\hat{\eta} = \hat{\eta}^+ + \hat{\eta}^-$  in (2.24) is always valid even for a flat bottom with  $\beta = 0$ , where the sum  $\hat{\eta}^+ + \hat{\eta}^-$  recovers the equilibrium solution by Longuet-Higgins & Stewart (1962).

As shown later, the analytical consideration of subharmonic wave-induced mass transport requires its velocity  $\tilde{u}$  or  $\hat{u}$ , which was not obtained in Liao *et al.* (2023). To derive that, substituting (2.21) into the second equation in (2.18) and retaining terms to order  $O(\beta)$  yields the solution for  $\hat{Q}$  under the off-resonance condition in intermediate depth

$$\hat{Q}(x) = \frac{-\hat{S}c_g}{gh\mu} \left\{ 1 + \frac{i\beta}{\mu} \left( \frac{2-3\mu-\mu^2}{1-\mu} \frac{d}{d\ln h} \ln \left( \frac{2c_g}{c} - \frac{1}{2} \right) - \frac{3-4\mu-\mu^2}{1-\mu} \frac{d}{d\ln h} \ln c_g \right. \right. \\ \left. \left. - 1 + \frac{\mu-2}{1-\mu} \frac{d}{d\ln h} \ln \mu \right) + O(\beta^2) \right\}. \quad (2.25)$$

Similarly, substituting (2.23) into the second equation in (2.18) yields the leading-order solution in shallow water

$$\hat{Q}(x) = \frac{\hat{S}}{c_g} + \sqrt{gh} \left[ \hat{\eta}_f^+(x_0) \hat{\eta}_h^+(x, x_0) - \hat{\eta}_f^-(x_0) \hat{\eta}_h^-(x, x_0) + \int_{x_0}^x \frac{k_l^2}{2ik_f} \frac{\hat{S}}{gh} [\hat{\eta}_h^+(x, y) \right. \\ \left. + \hat{\eta}_h^-(x, y)] dy \right]. \quad (2.26)$$

As reflected in (2.18),  $\hat{Q}$  is the combined effect of the direct response of the subharmonic volume flux to the forcing of radiation stress gradient  $\partial \hat{S} / \partial x$  and the volume flux carried by subharmonic waves (the  $\partial \hat{\eta} / \partial x$  term). At leading order, the former leads to the first term  $\hat{S} / c_g$  on the right-hand side of (2.26), while the latter is essentially multiplying the forward and backward propagating subharmonic waves in (2.23) with their corresponding phase speeds  $\sqrt{gh}$  and  $-\sqrt{gh}$ .

Combining (2.17) and (2.26) yields the complex amplitude of subharmonic orbital velocity  $\hat{u}$

$$\hat{u}(x) = \frac{\hat{Q} - \hat{E}/c}{h}. \quad (2.27)$$

As a special case, consider a bichromatic wave system over a flat bed at a water depth deep for the primary waves but shallow for the wave group. Substituting  $\beta = 0$ ,  $\hat{E} = g\hat{a}_n\hat{a}_{n-l}^* \exp[i(\int_{x_0}^x k_l dx' - \omega_l t)]$  (2.12),  $\hat{S} = \hat{E}((2c_g/c) - (1/2))$  and the deep-water relationship  $c_g = 1/2c = g/(2\omega_p)$  into (2.25), and then into (2.27) yields

$$\hat{u}(x) = -\frac{\omega_p}{2h} \frac{\hat{a}_n\hat{a}_{n-l}^*}{1 - 1/(4k_ph)} \exp\left(i \int_{x_0}^x k_l dx'\right), \quad (2.28)$$

which is equivalent to (2.3) in van den Bremer *et al.* (2019).

## 2.2. Eulerian transport

### 2.2.1. Generalised theory

In an Eulerian coordinate system, the wave-induced mass transport in homogeneous media with unit  $\rho$  is defined as

$$M(x, t) = \int_{-h}^{\eta} u dz = \int_{-h}^0 u dz + \int_0^{\eta} u dz. \quad (2.29)$$

The horizontal velocity  $u$  can be expanded vertically around  $z = 0$  as

$$u(x, t) = u|_{z=0} + z \left. \frac{\partial u}{\partial z} \right|_{z=0} + \frac{1}{2} z^2 \left. \frac{\partial^2 u}{\partial z^2} \right|_{z=0} + \dots \quad (2.30)$$

Substituting (2.30) into (2.29) yields

$$M(x, t) = \int_{-h}^0 u dz + u_0 \eta + \frac{1}{2} \left. \frac{\partial u}{\partial z} \right|_{z=0} \eta^2 + \frac{1}{6} \left. \frac{\partial^2 u}{\partial z^2} \right|_{z=0} \eta^3 + \dots, \quad (2.31)$$

where the subscript 0 indicates evaluation at  $z = 0$

Substituting the asymptotic expansion of  $u$  and  $\eta$  in (2.1) into (2.31) yields  $M = M^{(1)} + M^{(2)} + M^{(3)} + M^{(4)} + \dots$ , where the superscript  $(i)$  denotes the variable at the order of  $O(\varepsilon^i)$ , i.e.

$$M^{(1)}(x, t) = \int_{-h}^0 u^{(1)} dz, \quad (2.32a)$$

$$M^{(2)}(x, t) = \int_{-h}^0 u^{(2)} dz + u_0^{(1)} \eta^{(1)}, \quad (2.32b)$$

$$M^{(3)}(x, t) = \int_{-h}^0 u^{(3)} dz + u_0^{(1)} \eta^{(2)} + u_0^{(2)} \eta^{(1)} + \frac{1}{2} \left. \frac{\partial u^{(1)}}{\partial z} \right|_{z=0} [\eta^{(1)}]^2, \quad (2.32c)$$

$$\begin{aligned} M^{(4)}(x, t) = & \int_{-h}^0 u^{(4)} dz + u_0^{(1)} \eta^{(3)} + u_0^{(2)} \eta^{(2)} + u_0^{(3)} \eta^{(1)} + \frac{1}{2} \left. \frac{\partial u^{(2)}}{\partial z} \right|_{z=0} [\eta^{(1)}]^2 \\ & + \left. \frac{\partial u^{(1)}}{\partial z} \right|_{z=0} \eta^{(1)} \eta^{(2)} + \frac{1}{6} \left. \frac{\partial^2 u^{(1)}}{\partial z^2} \right|_{z=0} [\eta^{(1)}]^3. \end{aligned} \quad (2.32d)$$

Our goal is to obtain the time-averaged mass transport  $\bar{M}$  at each order and seek terms involving the second-order subharmonic velocity  $\tilde{u}$  to assess its contribution. Physically, an Eulerian velocity of order  $O(\varepsilon^3)$  such as  $u^{(3)}$  and  $u^{(4)}$  will depend on  $\tilde{u}$  and so will the mass transport terms involving them. This dependence of mass transport on  $\tilde{u}$ , however, is dynamic rather than kinematic. The latter may be defined as the difference in the drift velocity of a Lagrangian particle after subtracting  $\tilde{u}$  from the background flow, whereby the former requires the derivation of the change in flow field at higher orders due to subtracting  $\tilde{u}$  using the momentum equations and boundary conditions. The present study focuses on the kinematic contribution of subharmonic waves to the mass transport, thereby  $u^{(3)}$  and  $u^{(4)}$  are neglected hereinafter. The subharmonic-induced mass transport solution will be similar to the kinematic Stokes drift velocity (1.2) without the accompanying second-order subharmonic return flow.

To proceed, we will first consider a more general wave velocity field without the assumptions  $\alpha = O(\varepsilon) \ll 1$ ,  $k_l h = O(\alpha k h) = O(\varepsilon k h) \ll 1$  to derive the result of subharmonic-induced mass transport and then simplify it to the different parameter regimes. The first-order horizontal velocity  $u^{(1)}$  takes the same expression as in (2.4). The following general form is now adopted for subharmonic velocity  $\tilde{u}$  contributing to  $u^{(2)}$  as suggested by the solution of subharmonic velocity obtained in Longuet-Higgins & Stewart (1962) ((3.10) therein):

$$\begin{cases} u^{(2)} = \tilde{u} + (\text{superharmonic terms}), \\ \tilde{u}(x, z, t) = \sum_{n,m} \hat{U}_{m,n} \frac{\cosh[k_{m,n}(z+h)]}{\cosh k_{m,n}h} \exp i\theta_{m,n}, \end{cases} \quad (2.33)$$

with

$$\begin{cases} \theta_{m,n} = k_{m,n}x - \omega_{m,n}t, \\ k_{m,n} = k_m - k_n, \\ \omega_{m,n} = \omega_m - \omega_n. \end{cases} \quad (2.34)$$

Both indices  $n$  and  $m$  were summed over the same frequency domain of  $u^{(1)}$ . Substituting (2.4) into (2.32a) yields  $M^{(1)}$

$$M^{(1)} = \sum_m \frac{\hat{u}_m}{k_m} \tanh k_m h \exp i\theta_m. \quad (2.35)$$

After obtaining  $M^{(i)}$ ,  $\eta^{(i)}$  is needed for deriving  $M^{(j)}$  ( $j > i$ ) and can be obtained from the continuity equation as

$$\eta^{(i)} = - \int \frac{\partial M^{(i)}}{\partial x} dt. \quad (2.36)$$

Substituting (2.35) into (2.36) yields  $\eta^{(1)}$

$$\eta^{(1)} = \sum_m \frac{\hat{u}_m}{\omega_m} \tanh k_m h \exp i\theta_m, \quad (2.37)$$

which together with  $u^{(2)}$  in (2.33) and  $u^{(1)}$  in (2.4), is further substituted into (2.31b) to yield  $M^{(2)}$ . Repeating this process, the terms in  $M^{(4)}$  involving subharmonic velocity  $\tilde{u}$  can be identified

$$\begin{aligned} M^{(4)}(x, t) &= u_0^{(1)} \underbrace{\int \frac{\partial}{\partial x} \left[ u_0^{(1)} \int \left( \int_{-h}^0 \frac{\partial \tilde{u}}{\partial x} dz \right) dt - \tilde{u}_0 \eta^{(1)} \right]}_{u_0^{(1)} \eta^{(3)}} \underbrace{dt - u_0^{(2)} \int \frac{\partial}{\partial x} \left( \int_{-h}^0 \tilde{u} dz + u_0^{(1)} \eta^{(1)} \right) dt}_{u_0^{(2)} \eta^{(2)}} \\ &\quad + \frac{1}{2} \frac{\partial \tilde{u}}{\partial z} \Big|_{z=0} [\eta^{(1)}]^2 - \frac{\partial u^{(1)}}{\partial z} \Big|_{z=0} \eta^{(1)} \int \frac{\partial}{\partial x} \left( \int_{-h}^0 \tilde{u} dz \right) dt + (\text{terms without } \tilde{u}). \end{aligned} \quad (2.38)$$

Notice that the first term on the right-hand side of (2.38) is part of the term  $u_0^{(1)} \eta^{(3)}$ , accounting for the interaction of  $u_0^{(1)}$  with  $\tilde{u}$  through the component of  $\eta^{(3)}$ . The phase

average of this term turns out to be non-zero and therefore contributes to the mass transport.

Invoking (2.4) for  $u^{(1)}$  and (2.33) for  $\tilde{u}$  and (2.37) for  $\eta^{(1)}$ , the expression of (2.38) for  $\bar{M}^{(4)}$  can be worked out. Maintaining only the steady terms involving the subharmonic velocity  $\hat{U}_{m,n}$  yields

$$\bar{M}^{(4)}(x) = \sum_{m,n} \underbrace{\frac{1}{2} \hat{U}_{m,n} \hat{U}_{m,n}^* \frac{\tanh k_{m,n} h}{\omega_{m,n}}}_{\text{Term I}} + \underbrace{\frac{1}{4} D_{m,n} \hat{u}_m^* \hat{u}_n \hat{U}_{m,n} h}_{\text{Term II}}, \quad (2.39)$$

with

$$\begin{aligned} D_{m,n} = & \left( \frac{k_{m,n}}{\omega_{m,n}} + \frac{k_n}{\omega_n} \right) \frac{k_m}{\omega_m} \frac{\tanh k_m h}{k_m h} + \left( \frac{k_{m,n}}{\omega_{m,n}} + \frac{k_m}{\omega_m} \right) \frac{k_n}{\omega_n} \frac{\tanh k_n h}{k_n h} \\ & + \left( \frac{k_m}{\omega_m} + \frac{k_n}{\omega_n} \right) \frac{k_{m,n}}{\omega_{m,n}} \frac{\tanh k_{m,n} h}{k_{m,n} h} \\ & + \left[ \left( \frac{k_n}{\omega_m} + \frac{k_m}{\omega_n} \right) \frac{k_{m,n}}{\omega_{m,n}} + \frac{k_{m,n}^2}{\omega_m \omega_n} \right] \frac{\tanh k_m h \tanh k_n h \tanh k_{m,n} h}{k_{m,n} h}. \end{aligned} \quad (2.40)$$

Equation (2.39) is a generalised subharmonic-induced mass transport solution for arbitrary depth and bandwidth and can be further simplified depending on the short wave relative depth ( $k_n h$ ,  $k_m h$ ), subharmonic wave relative depth ( $k_{m,n} h$ ) and bandwidth  $\alpha$ . Detailed derivations are provided in [Appendix A](#).

Noteworthily, the correlation between subharmonic velocity and surface elevation  $\overline{\tilde{u}_0 \tilde{\eta}}$  only contributes partly to  $\bar{M}^{(4)}$  through the  $u_0^{(2)} \eta^{(2)}$  term in (2.31). In fact, considering  $\overline{\tilde{u}_0 \tilde{\eta}}$  only yields

$$\overline{\tilde{u}_0 \tilde{\eta}} = \sum_{m,n} \frac{1}{2} \hat{U}_{m,n} \hat{U}_{m,n}^* \frac{\tanh k_{m,n} h}{\omega_{m,n}} + \frac{1}{4} \frac{k_{m,n}}{\omega_{m,n}} \left( \frac{\tanh k_m h}{\omega_m h} + \frac{\tanh k_n h}{\omega_n h} \right) \hat{u}_m^* \hat{u}_n \hat{U}_{m,n} h, \quad (2.41)$$

where we find the entire Term I in (2.39) but only part of the Term II.

### 2.2.2. Narrow-banded waves with wave groups long compared with the depth

Among the simplifications of (2.39) presented in [Appendix A](#), the scenario of narrow-banded waves with wave groups long compared with the depth, i.e.

$$\alpha \ll 1, \quad |k_{m,n}| h \ll 1, \quad (2.42)$$

is consistent with the theory in § 2.1 and thus of particular interest in this study. The corresponding simplified (2.39) is given by (A22). Normalising  $c$  and  $c_g$  with  $\sqrt{gh}$  yields an alternative form of (A22)

$$\bar{M}^{(4)}(x) = \underbrace{\frac{\overline{\tilde{u}^2} h}{c_g}}_{\text{Term I}} + \underbrace{f(k_p h) \frac{\left[ u^{(1)}|_{z=0} \right]^2 \tilde{u}}{g}}_{\text{Term II}}, \quad (2.43)$$

where the function  $f(k_p h)$  is

$$f(k_p h) = \frac{3 \sinh 2k_p h + 6k_p h \cosh^2 k_p h + 2k_p h \sinh^2 k_p h}{\sinh 2k_p h + 2k_p h}. \quad (2.44)$$

The function  $f(k_ph)$  increases monotonically with  $k_ph$ . For short waves in deep water  $k_ph \gg 1$ ,  $f(k_ph)$  approaches  $\sim 3 + 4\omega_p^2 h/g$  asymptotically; for shallow water  $k_ph \ll 1$ ,  $f(k_ph) = 3 + O(k_p^2 h^2)$ . Note that, in deep water  $k_ph \gg 1$ , the shallow-water regime for subharmonic wave ( $|k_{m,n}|h \ll 1$ ) is only valid for the subharmonic component with low enough frequencies or when the bandwidth  $\alpha$  is so small that  $|k_{m,n}|h = O(\alpha k_ph) \ll 1$ .

### 2.2.3. Second definition

Alternatively, let  $z = \eta_c(x)$  and  $z = \eta_t(x)$  be the wave crest and trough, i.e. the local maximum and minimum values of  $\eta$ , respectively. Below  $z = \eta_c(x)$  the time-averaged Eulerian velocity is zero while between  $z = \eta_c(x)$  and  $z = \eta_t(x)$  the velocity observed at a fixed height is intermittently zero similar to (1.4). The subharmonic wave-induced mass transport can be defined as the contribution of  $\tilde{u}$  to the integral

$$\bar{M}(x) = \int_{\eta_t}^{\eta_c} \bar{u} dz. \quad (2.45)$$

This definition, however, is more difficult to analyse than (2.29) despite the fact that both should yield the same results. As the first step, substituting the expansion of  $u$  into (2.45) yields

$$\bar{M} = \int_{\eta_t}^{\eta_c} \overline{u^{(1)} + u^{(2)} + u^{(3)}} dz + O(\varepsilon^5). \quad (2.46)$$

Invoking  $u^{(2)}$  in (2.33), (2.46) becomes

$$\bar{M} = \int_{\eta_t}^{\eta_c} \overline{u^{(1)}} + \bar{\tilde{u}} dz + (\text{terms without } \tilde{u}) + O(\varepsilon^5). \quad (2.47)$$

As shown later,  $\int_{\eta_t}^{\eta_c} \bar{\tilde{u}} dz$  can be estimated from experimental data, which implies  $\int_{\eta_t}^{\eta_c} \bar{\tilde{u}} dz$  is equal to  $\bar{\tilde{u}}\bar{\eta}$  although we do not seek its proof in this work. However, it remains challenging to analyse either analytically or experimentally the contribution of  $\tilde{u}$  to  $\int_{\eta_t}^{\eta_c} \overline{u^{(1)}} dz$  through terms analogous to  $u_0^{(1)}\eta^{(3)}$  in (2.31).

## 2.3. Lagrangian transport

In the Lagrangian system, the Lagrangian velocity  $\mathbf{u}_L(t) = [u_L(t), w_L(t)]$  describes the velocity of a moving particle passively following the background Eulerian velocity  $\mathbf{u}(x, z, t) = [u(x, z, t), w(x, z, t)]$ . The mass transport is obtained by integrating vertically the steady component in  $u_L$ , i.e.  $\bar{M} = \int_{-h}^0 \overline{u_L} dz$ . Compared with the bulk transport  $\bar{M}$  obtained in an Eulerian system,  $\overline{u_L}$  offers more information on the vertical distribution of how fluid particles at different depths physically drift.

### 2.3.1. Generalised theory

The horizontal and vertical displacements of a fluid particle released from  $\mathbf{r}_0 = (x_0, z_0)$  at  $t = 0$  underneath waves  $\Delta \mathbf{r}(t) = [\Delta x(t), \Delta z(t)]$  are given by the time integration of its Lagrangian velocity  $\mathbf{u}_L(t)$

$$\Delta \mathbf{r}(t) = \int \mathbf{u}_L(t) dt, \quad (2.48)$$

where  $\mathbf{u}_L(t)$  is obtained by querying the Eulerian velocity field following the particle coordinate in real time, i.e.

$$\mathbf{u}_L(t) = \mathbf{u}(\mathbf{r}_0 + \Delta \mathbf{r}(t), t). \quad (2.49)$$

The right-hand side of (2.49) can be expanded around  $\mathbf{r}_0$  using Taylor series as

$$\mathbf{u}_L(t) = \left\{ \left( 1 + \Delta \mathbf{r} \cdot \nabla + \frac{1}{2} [\Delta \mathbf{r} \cdot (\Delta \mathbf{r} \cdot \mathbf{H})] + \dots \right) \mathbf{u} \right\}_{(\mathbf{r}_0, t)}, \quad (2.50)$$

$$\nabla = \left( \frac{\partial}{\partial x}, \frac{\partial}{\partial z} \right), \quad \mathbf{H} = \begin{bmatrix} \frac{\partial^2}{\partial x^2} & \frac{\partial^2}{\partial x \partial z} \\ \frac{\partial^2}{\partial x \partial z} & \frac{\partial^2}{\partial z^2} \end{bmatrix}$$

where the subscript coordinates  $(\mathbf{r}_0, t)$  will be omitted hereinafter.

Applying Stokes expansion in  $\varepsilon$  to  $\mathbf{u}$ ,  $\mathbf{u}_L$  and  $\Delta \mathbf{r}$  and then substituting them into (2.50) yields

$$\mathbf{u}_L^{(1)}(x, z, t) = \mathbf{u}^{(1)}, \quad (2.51a)$$

$$\mathbf{u}_L^{(2)}(x, z, t) = \mathbf{u}^{(2)} + \Delta \mathbf{r}^{(1)} \cdot \nabla \mathbf{u}^{(1)}, \quad (2.51b)$$

$$\mathbf{u}_L^{(3)}(x, z, t) = \mathbf{u}^{(3)} + \Delta \mathbf{r}^{(1)} \cdot \nabla \mathbf{u}^{(2)} + \Delta \mathbf{r}^{(2)} \cdot \nabla \mathbf{u}^{(1)} + \frac{1}{2} [\Delta \mathbf{r}^{(1)} \cdot (\Delta \mathbf{r}^{(1)} \cdot \mathbf{H})] \mathbf{u}^{(1)}, \quad (2.51c)$$

$$\begin{aligned} \mathbf{u}_L^{(4)}(x, z, t) = & \mathbf{u}^{(4)} + \Delta \mathbf{r}^{(1)} \cdot \nabla \mathbf{u}^{(3)} + \Delta \mathbf{r}^{(2)} \cdot \nabla \mathbf{u}^{(2)} + \Delta \mathbf{r}^{(3)} \cdot \nabla \mathbf{u}^{(1)} \\ & + \frac{1}{2} [\Delta \mathbf{r}^{(1)} \cdot (\Delta \mathbf{r}^{(1)} \cdot \mathbf{H})] \mathbf{u}^{(2)} + [\Delta \mathbf{r}^{(1)} \cdot (\Delta \mathbf{r}^{(2)} \cdot \mathbf{H})] \mathbf{u}^{(1)} \\ & + \frac{1}{6} \left( [\Delta x^{(1)}]^3 \frac{\partial^3}{\partial x^3} + 3[\Delta x^{(1)}]^2 \Delta z^{(1)} \frac{\partial^3}{\partial x^2 \partial z} + 3[\Delta z^{(1)}]^2 \Delta x^{(1)} \frac{\partial^3}{\partial x \partial z^2} \right. \\ & \left. + [\Delta z^{(1)}]^3 \frac{\partial^3}{\partial z^3} \right) \mathbf{u}^{(1)}. \end{aligned} \quad (2.51d)$$

The horizontal component of  $\mathbf{u}^{(1)} = [u^{(1)}, w^{(1)}]$  can be found from (2.4), while the vertical component  $w^{(1)}$  can be obtained by integrating the continuity equation vertically

$$w^{(1)}(x, z, t) = w^{(1)}(x, -h, t) - \int_{-h}^z \frac{\partial}{\partial x} u^{(1)}(x, z', t) dz', \quad (2.52)$$

where  $w^{(1)}(x, -h, t)$  is the bottom vertical velocity, which is of  $O(\varepsilon h_x)$  due to kinematic condition  $w = -uh_x$  at the bottom  $z = -h$ . Because  $|h_x| \ll O(\varepsilon kh)$ , for  $kh = O(1)$  we have  $w^{(1)}(x, -h, t) = O(\varepsilon h_x) \ll O(\varepsilon^2)$  while for  $kh \gg 1$  the bottom effect is neglected. Therefore,  $w^{(1)}(x, -h, t)$  will be excluded in both  $w^{(1)}$  and  $w^{(2)}$ . Substituting (2.4) into (2.52) and taking  $w^{(1)}(x, -h, t) = 0$  yields

$$w^{(1)}(x, z, t) = \sum_{n=n_1}^{n_1+N} -i \hat{u}_n(x) \frac{\sinh[k_n(z+h)]}{\cosh k_n h} \exp i \theta_n. \quad (2.53)$$

Substituting (2.4) and (2.53) into  $\mathbf{u}^{(1)} = [u^{(1)}, w^{(1)}]$  and then into (2.51a) yields  $\mathbf{u}_L^{(1)}$ . Then the  $\Delta \mathbf{r}^{(1)}$  can be obtained following  $\Delta \mathbf{r}^{(i)} = \int \mathbf{u}_L^{(i)}(t) dt$ . After  $\Delta \mathbf{r}^{(1)}$  is obtained,

$\mathbf{u}^{(2)}$  is still needed to evaluate  $\mathbf{u}_L^{(2)}$ . The horizontal component of  $\mathbf{u}^{(2)} = [u^{(2)}, w^{(2)}]$  can be found from (2.33), while the vertical component  $w^{(2)}$  is obtained similar to  $w^{(1)}$  as

$$\begin{cases} w^{(2)} = \tilde{w} + (\text{superharmonic terms}) \\ \tilde{w}(x, z, t) = \sum_{n,m} -i\hat{U}_{m,n} \frac{\sinh[k_{m,n}(z+h)]}{\cosh k_{m,n}h} \exp i\theta_{m,n} \end{cases} \quad (2.54)$$

Substituting  $\mathbf{u}^{(2)} = [u^{(2)}, w^{(2)}]$ ,  $\Delta \mathbf{r}^{(1)}$  and  $\mathbf{u}^{(1)}$  into (2.50) yields  $\mathbf{u}_L^{(2)}$  and, by  $\Delta \mathbf{r}^{(i)} = \int \mathbf{u}_L^{(i)}(t)dt$ ,  $\Delta \mathbf{r}^{(2)}$ . Repeating this process, the expression of  $\mathbf{u}_L^{(4)}$  can be worked out after lengthy algebra. Since we are interested in the resultant  $u_L^{(4)}$  involving  $\hat{U}_{m,n}$ , it will be useful to write out the expression of  $u_L^{(4)}$

$$\begin{aligned} u_L^{(4)}(x, z, t) = & \Delta x^{(2)} \frac{\partial \tilde{u}}{\partial x} + \Delta z^{(2)} \frac{\partial \tilde{u}}{\partial z} + \Delta x^{(1)} \Delta x^{(2)} \frac{\partial^2 u^{(1)}}{\partial x^2} \\ & + [\Delta x^{(1)} \Delta z^{(2)} + \Delta z^{(1)} \Delta x^{(2)}] \frac{\partial^2 u^{(1)}}{\partial x \partial z} + \Delta z^{(1)} \Delta z^{(2)} \frac{\partial^2 u^{(1)}}{\partial z^2} + \Delta x^{(3)} \frac{\partial u^{(1)}}{\partial x} \\ & + \Delta z^{(3)} \frac{\partial u^{(1)}}{\partial z} + \frac{1}{2} [\Delta x^{(1)}]^2 \frac{\partial^2 \tilde{u}}{\partial x^2} + \Delta x^{(1)} \Delta z^{(1)} \frac{\partial^2 \tilde{u}}{\partial x \partial z} + \frac{1}{2} [\Delta z^{(1)}]^2 \frac{\partial^2 \tilde{u}}{\partial z^2} \\ & + (\text{terms without } \tilde{u} \text{ or } \tilde{w}), \end{aligned} \quad (2.55)$$

and evaluate each part separately. Note that in (2.55) the exclusion of terms without  $\tilde{u}$  or  $\tilde{w}$  were not exhausted (e.g. expanding  $\Delta x^{(2)}$  in  $\Delta x^{(1)} \Delta x^{(2)} (\partial^2 u^{(1)}) / (\partial x^2)$  also generates those terms). The steady terms in each part are

$$\begin{aligned} \overline{\Delta x^{(2)} \frac{\partial \tilde{u}}{\partial x} + \Delta z^{(2)} \frac{\partial \tilde{u}}{\partial z}} = & \sum_{m,n} \hat{U}_{m,n} \hat{U}_{m,n}^* \frac{k_{m,n}}{\omega_{m,n}} \frac{\cosh[2k_{m,n}(z+h)]}{2 \cosh^2 k_{m,n}h} \\ & + \frac{B_{m,n}^I \hat{u}_m^* \hat{u}_n \hat{U}_{m,n}}{4 \cosh k_m h \cosh k_n h \cosh k_{m,n} h} + (\text{terms without } \tilde{u} \text{ or } \tilde{w}), \end{aligned} \quad (2.56)$$

$$\begin{aligned} \overline{\Delta x^{(3)} \frac{\partial u^{(1)}}{\partial x} + \Delta z^{(3)} \frac{\partial u^{(1)}}{\partial z}} = & \sum_{m,n} \frac{B_{m,n}^{II} \hat{u}_m^* \hat{u}_n \hat{U}_{m,n}}{4 \cosh k_m h \cosh k_n h \cosh k_{m,n} h} \\ & + (\text{terms without } \tilde{u} \text{ or } \tilde{w}), \end{aligned} \quad (2.57)$$

$$\begin{aligned} \overline{\Delta x^{(1)} \Delta x^{(2)} \frac{\partial^2 u^{(1)}}{\partial x^2} + [\Delta x^{(1)} \Delta z^{(2)} + \Delta z^{(1)} \Delta x^{(2)}] \frac{\partial^2 u^{(1)}}{\partial x \partial z} + \Delta z^{(1)} \Delta z^{(2)} \frac{\partial^2 u^{(1)}}{\partial z^2}} \\ = \sum_{m,n} \frac{B_{m,n}^{III} \hat{u}_m^* \hat{u}_n \hat{U}_{m,n}}{4 \cosh k_m h \cosh k_n h \cosh k_{m,n} h} + (\text{terms without } \tilde{u} \text{ or } \tilde{w}), \end{aligned} \quad (2.58)$$

$$\begin{aligned} \overline{\frac{1}{2} [\Delta x^{(1)}]^2 \frac{\partial^2 \tilde{u}}{\partial x^2} + \Delta x^{(1)} \Delta z^{(1)} \frac{\partial^2 \tilde{u}}{\partial x \partial z} + \frac{1}{2} [\Delta z^{(1)}]^2 \frac{\partial^2 \tilde{u}}{\partial z^2}} \\ = \sum_{m,n} \frac{B_{m,n}^{III} \hat{u}_m^* \hat{u}_n \hat{U}_{m,n}}{4 \cosh k_m h \cosh k_n h \cosh k_{m,n} h} + (\text{terms without } \tilde{u} \text{ or } \tilde{w}), \end{aligned} \quad (2.59)$$

with the coefficients  $B_{m,n}^I$  to  $B_{m,n}^{IIII}$

$$\begin{bmatrix} B_{m,n}^I \\ B_{m,n}^{II} \\ B_{m,n}^{III} \\ B_{m,n}^{IIII} \end{bmatrix} = \begin{bmatrix} \frac{k_{m,n}}{\omega_{m,n}} \left\{ \frac{k_n}{\omega_m} \cosh [2k_n(z+h)] + \frac{k_m}{\omega_n} \cosh [2k_m(z+h)] \right\} \\ \frac{k_m k_n}{\omega_m \omega_n} \frac{\{\omega \cosh [2k(z+h)]\}_{m,n}}{\omega_{m,n}} - \frac{k_{m,n}^2}{\omega_m \omega_n} \cosh [2k_{m,n}(z+h)] \\ - \frac{k_{m,n}^2}{\omega_m \omega_n} \cosh [2k_{m,n}(z+h)] \\ \frac{\{\omega k^2 \cosh [2k(z+h)]\}_{m,n}}{\omega_m \omega_n \omega_{m,n}} \end{bmatrix}, \quad (2.60)$$

where all the subscripts  $m, n$  on the right-hand side denote the difference between the  $m$ th and  $n$ th frequency components. Collecting (2.56)–(2.59) yields  $\overline{u_L^{(4)}}$

$$\begin{aligned} \overline{u_L^{(4)}}(x, z) = \sum_{m,n} \underbrace{\widehat{U}_{m,n} \widehat{U}_{m,n}^* \frac{k_{m,n}}{\omega_{m,n}} \frac{\cosh [2k_{m,n}(z+h)]}{2 \cosh^2 k_{m,n}h}}_{\text{Term I}} \\ + \underbrace{\frac{(B_{m,n}^I + B_{m,n}^{II} + B_{m,n}^{III} + B_{m,n}^{IIII}) \hat{u}_m^* \hat{u}_n \widehat{U}_{m,n}}{4 \cosh k_m h \cosh k_n h \cosh k_{m,n}h}}_{\text{Term II}}, \end{aligned} \quad (2.61)$$

and integrating  $\overline{u_L^{(4)}}$  vertically yields the mass transport  $\bar{M}^{(4)}(x) = \int_{-h}^0 \overline{u_L^{(4)}}(x, z) dz$

$$\bar{M}^{(4)}(x) = \sum_{m,n} \frac{1}{2} \widehat{U}_{m,n} \widehat{U}_{m,n}^* \frac{\tanh k_{m,n}h}{\omega_{m,n}} + \frac{1}{4} D_{m,n} \hat{u}_m^* \hat{u}_n \widehat{U}_{m,n}h, \quad (2.62)$$

with

$$\begin{aligned} D_{m,n} = & \left( \frac{1}{\omega_m} \frac{\tanh k_m h - \tanh k_{m,n}h}{h} + \frac{1}{\omega_n} \frac{\tanh k_n h + \tanh k_{m,n}h}{h} \right) \frac{k_{m,n}}{\omega_{m,n}} \\ & + \frac{k_m k_n}{\omega_m \omega_n} \left( \frac{\omega_m}{\omega_{m,n}} \frac{\tanh k_n h + \tanh k_{m,n}h}{k_m h} - \frac{\omega_n}{\omega_{m,n}} \frac{\tanh k_m h - \tanh k_{m,n}h}{k_n h} \right) \\ & - \frac{2k_{m,n}^2}{\omega_m \omega_n} \frac{\tanh k_m h - \tanh k_n h}{k_{m,n}h} \\ & + \frac{\omega_m k_m (\tanh k_n h + \tanh k_{m,n}h) - \omega_n k_n (\tanh k_m h - \tanh k_{m,n}h)}{\omega_m \omega_n \omega_{m,n}h}. \end{aligned} \quad (2.63)$$

Term I on the right-hand side of (2.62) is the same as in (2.39) obtained in Eulerian system. Also, both equations are equivalent for the coefficient  $D_{m,n}$  (see Appendix B for a proof). Therefore, the result of  $\bar{M}^{(4)}$  derived in the Lagrangian system (2.62) is consistent with that in the Eulerian system (2.39).

At the leading order, the mass transport is the sum of Term I and II, as labelled in (2.39) and (2.61). Term I originates from the term  $\overline{\int \mathbf{u}^{(2)} dt \cdot \nabla \mathbf{u}^{(2)}}$  and accounts for the net displacement solely due to the subharmonic motion (self-interaction), in analogy to the Stokes drift velocity due to the primary wave orbital motion. Term II takes the form of the weighted sum of all bispectral components of horizontal velocity skewness  $\text{Re}[\hat{u}_m^* \hat{u}_n \hat{U}_{m,n}]$  arising from the triad-difference interaction among two primary and one subharmonic components. Therefore, Term II may be regarded as the effect of subharmonic wave-induced skewness on the mass transport velocity. Note that these two terms do not necessarily balance with each other, and the residual of their sum has to be compensated at least partly by a steady component of  $u^{(4)}$  depending on the boundary conditions.

### 2.3.2. Narrow-banded waves with wave groups long compared with the depth

As shown in Appendix C, (2.61) for  $\overline{u_L^{(4)}}$  can be further simplified depending on the short wave relative depth ( $k_n h, k_m h$ ), subharmonic wave relative depth ( $k_{m,n} h$ ) and bandwidth  $\alpha$  similar to the simplifications to (2.39) in Appendix A. In the case of narrow-banded waves with wave groups that are long compared with the depth, equation (2.61) reduces to (C16), i.e.

$$\overline{u_L^{(4)}}(x, z) = \frac{\overline{\tilde{u}^2}}{c_g} + \zeta\left(k_p h, \frac{z}{h}\right) \frac{\left[u^{(1)}|_{z=0}\right]^2 \tilde{u}}{cc_g}, \quad (2.64)$$

where

$$\zeta\left(k_p h, \frac{z}{h}\right) = \left[\frac{5}{2} + \frac{k_p h}{\sinh 2k_p h} + 2k_p(z+h) \tanh[2k_p(z+h)]\right] \frac{\cosh[2k_p(z+h)]}{\cosh^2 k_p h}. \quad (2.65)$$

The second term of (2.64) is the product of the characteristic transport velocity  $\overline{[u^{(1)}|_{z=0}]^2 \tilde{u}}/(cc_g)$  and the depth-dependent coefficient  $\zeta$  which is a function of  $k_p h$  and the  $z/h$ , as shown in figure 3(a). For short waves in deep water  $k_p h \gg 1$ ,  $\zeta$  approaches  $(4\omega_p^2 h)/(g) \exp(2\omega_p^2 z/g)$  asymptotically; for shallow water  $k_p h \ll 1$ ,  $\zeta$  becomes  $3 + O(k_p^2 h^2)$ .

In (2.64) the weighting coefficient for all bispectral components of velocity skewness  $\text{Re}[\hat{u}_m^* \hat{u}_n \hat{U}_{m,n}]$  in (2.61) is the same and therefore Term II is simply proportional to  $\sum_{m,n} \text{Re}[\hat{u}_m^* \hat{u}_n \hat{U}_{m,n}] \propto \overline{[u^{(1)}|_{z=0}]^2 \tilde{u}}$ , which is non-zero due to phase coupling between the subharmonic wave and wave groups. As shown by Fiedler *et al.* (2019), the correlation  $\overline{\tilde{u}[u^{(1)}]^2}$  can be found through expanding the velocity skewness  $\overline{(u^{(1)} + \tilde{u})^3}$  as the contribution of subharmonic waves to the total velocity skewness.

For each pair of  $m$  and  $n$ , the ratio |Term I/Term II| in  $\bar{M}^{(4)}$  by (2.43) is given by

$$\frac{2gh}{f(k_p h)c_g} \frac{|\hat{U}_{m,n}|^2}{|\text{Re}[\hat{u}_m^* \hat{u}_n \hat{U}_{m,n}]|}, \quad (2.66)$$

which relies on a function of  $k_p h$  and the dependence of  $\hat{U}_{m,n}$  on  $\hat{u}_m^* \hat{u}_n$ . This dependence can be evaluated based on the equilibrium subharmonic wave solution on a flat bottom by Longuet-Higgins & Stewart (1962) and also the Green's function-based solution in § 2.1 and shown in figure 3(b). Both models indicate that Term I exceeds Term II for  $\mu < 0.36$  ( $k_p h < 0.72$ ), while the Green's function-based solution indicates decreasing critical  $\mu$  or  $k_p h$  as  $|\beta|$  increases and exceeds  $\sim 0.01$ . The relative importance of Term I

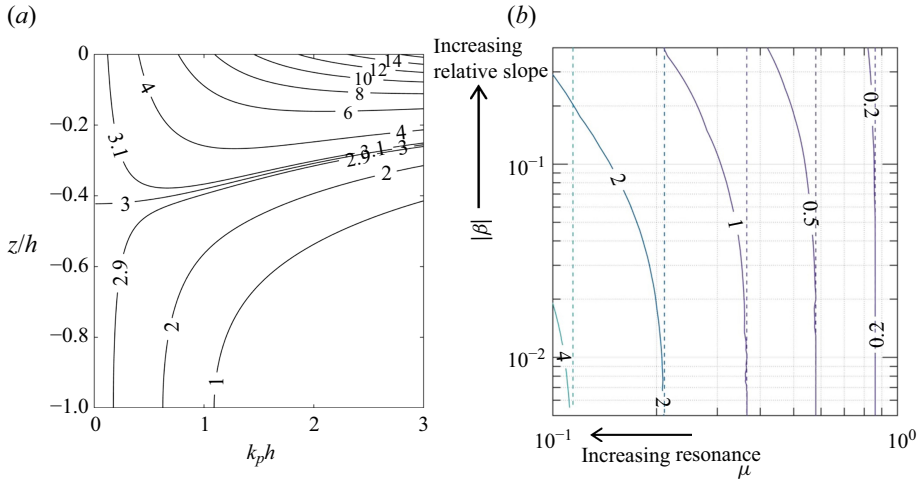


Figure 3. (a) Contour line of  $\zeta(k_p h, z/h)$  in (2.64) which describes the vertical distribution of the skewness-induced transport velocity due to subharmonics proportional to  $\overline{[u^{(1)}]_{z=0}^2 \tilde{u}} / (c c_g)$  at different short wave relative depths  $k_p h$ . (b) Theoretical prediction of (2.66), i.e. the ratio of Term I ('Stokes drift' type contribution) over Term II (velocity skewness contribution) for each pair of bichromatic waves in the subharmonic wave-induced mass transport given by (2.43). Dashed lines: flat bottom solution of Longuet-Higgins & Stewart (1962); solid lines: Green's function-based solution in § 2.1 based on Liao et al. (2023).  $\beta = h_x / (k_l h)$  is the relative bottom slope at wave group length scale,  $\mu = 1 - c_g^2 / (g h)$  is the parameter of departure from resonance.

increases with decreasing  $\mu$  due to increasing subharmonic wave energy during shoaling and with decreasing  $\beta$ . As  $\beta$  decreases, the predictions of the Green's function-based solution asymptotically approaches that of the equilibrium solution for a flat bottom. Notice that at given depth for equilibrium solution or small enough relative slope  $|\beta|$  this ratio becomes independent of  $\beta$  and hence subharmonic wavenumber  $k_l$ , suggesting that it also measures the ratio between the entire Term I over Term II.

## 2.4. Comparisons with GLOBEX experiment

### 2.4.1. Experimental set-up and data processing

The test series A of GLOBEX experiment (Ruessink et al. 2013) of unidirectional irregular waves normally incident onto a beach of 1/80 bed slope is employed to validate the model in § 2.1 for subharmonic surface elevation and velocity. Then, the theoretical model in §§ 2.2 and 2.3 is evaluated both analytically and experimentally to analyse the subharmonic wave-induced mass transport. Note that the experiment did not provide direct measurement of the kinematic effect of subharmonic wave-induced mass transport and therefore does not allow validation of the mass transport model proposed. This will be addressed in § 3 through comparative Lagrangian particle-tracking simulations.

Because the model in § 2.1 ignores the reflected subharmonic waves, the incident subharmonic surface elevation  $\tilde{\eta}$  and orbital velocity  $\tilde{u}$  were obtained using the weakly nonlinear method detailed in Appendix D. The significant wave height of the incoming subharmonic wave was then obtained as  $H_{lf} = 4\sqrt{(\tilde{\eta})^2}$ . The phase coupling between subharmonic waves and short wave groups (biphase) was calculated following Fiedler et al., (2019) as

$$\text{Biphase} = \tan^{-1} \left( \frac{\overline{\mathcal{H}\{\tilde{\eta}\} \mathcal{H}\{\eta^{(1)}\}^2}}{\tilde{\eta} [\eta^{(1)}]^2} \right), \quad (2.67)$$

where  $\mathcal{H}\{\cdot\}$  denotes the Hilbert transform and  $\eta^{(1)}$  the short wave surface elevation with frequency  $> 0.5/T_p$ .

To calculate the subharmonic wave-induced time-averaged velocity  $\bar{u}$  between wave crest  $z = \eta_c$  and trough  $z = \eta_t$  described in § 2.2.3, the incident subharmonic orbital velocity  $\tilde{u}$  measured at a fixed height above the bed was assumed to be uniform throughout the water column. At each cross-shore location with velocity measurements, 21 equidistant points from  $z = \eta_t$  to  $z = \eta_c$  were defined and at each point  $\tilde{u}$  is assigned with the simultaneous value of the  $\tilde{u}$  measured for the timepoints when it is below the free surface and otherwise zero. Time averaging the resultant  $\tilde{u}$  at the defined points yields the  $\bar{u}$  between the wave crest and trough.

To experimentally evaluate (2.43),  $\bar{u}^2$  is calculated from the incident subharmonic  $\tilde{u}$  while  $\overline{\tilde{u}[u^{(1)}|_{z=0}]^2}$  is evaluated using the measured  $\tilde{u}[u^{(1)}]^2$  at  $z_p + h$  above the bed according to

$$\overline{\tilde{u}[u^{(1)}|_{z=0}]^2} = \left\{ \overline{\tilde{u}[u^{(1)}]^2} \right\} \bigg|_{z=z_p} \frac{\cosh^2 k_p h}{\cosh^2 k_p (z_p + h)}. \quad (2.68)$$

#### 2.4.2. Validation of theoretical model for subharmonic wave

Figure 4(a–c) shows the flume set-up, significant wave height of the primary wave and the incoming subharmonic wave of A3 case of GLOBEX experiment. In figure 4(c), also shown is the theoretical wave height of subharmonic waves forced by wave groups,  $H_{lf} = 4\sqrt{\sum(\hat{\eta}_l \hat{\eta}_l^*/2)}$ , where the complex amplitude of subharmonic wave  $\hat{\eta}_l$  is given by (2.23). The theory predicted the observed growth of group-forced subharmonic waves in the shoaling zone and the outer surf zone very well, but overpredicted the observation in the inner surf zone. The overprediction in the surf zone is likely due to drastic modification of the phase of group forcing by a breaking process not included in the model (figure 4d), which is crucial for capturing the wave height decay in the inner surf zone (Liao *et al.* 2023).

The subharmonic wave-induced time-averaged velocity  $\bar{u}$  between wave crest  $z = \eta_c$  and trough  $z = \eta_t$  is illustrated in figure 4(e). Below the wave trough  $z = \eta_t$ , the oscillatory subharmonic wave leads to a zero time-averaged velocity  $\bar{u}$ . In the shoaling zone and outer surf zone,  $\bar{u}$  is negative near the wave crest  $z = \eta_c$  but positive near the wave trough  $z = \eta_t$ . This is because only the largest waves in the wave train can achieve the crest, when the subharmonic wave troughs and backward orbital velocity occurs since the group-forced subharmonic wave is in anti-phase with the wave group. The dominant forward velocity near the subharmonic wave trough leads to a net positive contribution of the term  $\int_{\eta_t}^{\eta_c} \bar{u} dz$  to the mass transport (2.47), which increases with decreasing depth towards the shore. In the inner surf zone, the negative velocity near the surface becomes positive, due to the transition from anti-phase to in-phase coupling between the subharmonic wave and wave groups (figure 4d). Although the model is no longer accurate for  $x > 70$  m in this region, the  $\bar{u}$  value evaluated from experimental measurements still offers insights into the mass transport, especially the effect of growing subharmonic waves and decaying short waves.

Figure 5 compares the measured and theoretically predicted mass transport component  $\rho \bar{u} \bar{\eta}$  in the shoaling zone. In all three cases, the theoretical predictions agree with the observations very well, validating the model in § 2.1 for subharmonic surface elevation and velocity. Noteworthy, the experimental results of the term  $\int_{\eta_t}^{\eta_c} \bar{u} dz$  are nearly identical to  $\bar{u} \bar{\eta}$ , suggesting that  $\int_{\eta_t}^{\eta_c} \bar{u} dz = \bar{u} \bar{\eta}$  although a theoretical demonstration is desired.

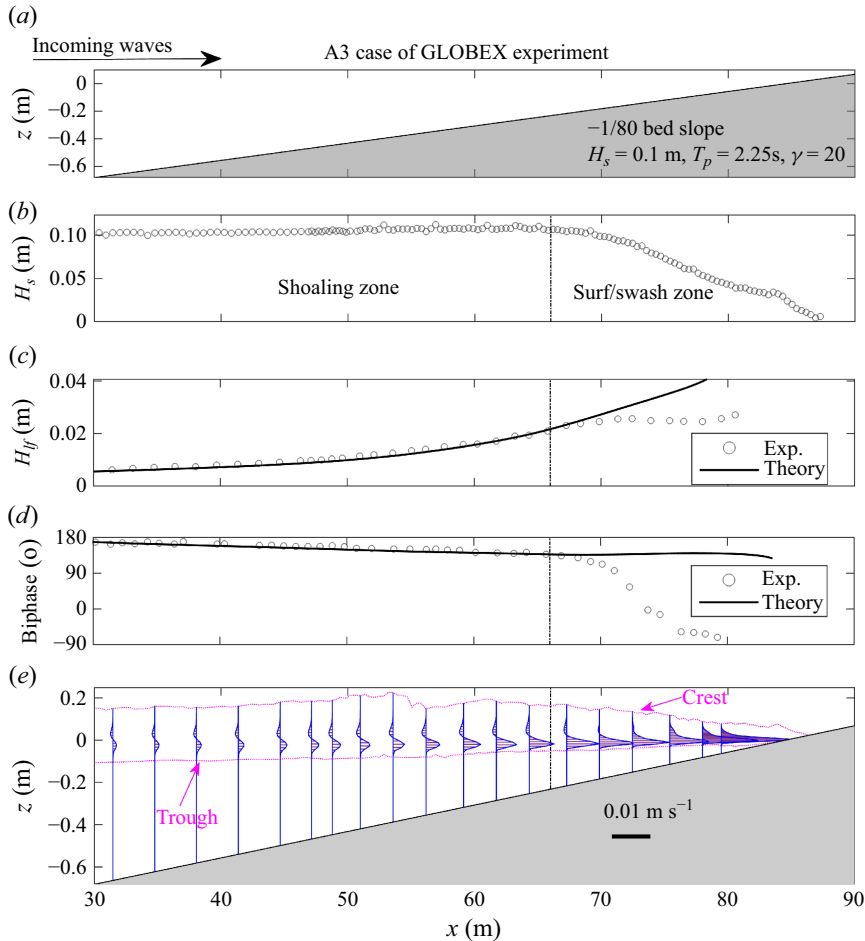


Figure 4. (a) Numerical flume set-up and wave conditions of Case A3 in the GLOBEX experiment. Significant wave height of (b) short wave (c) incident subharmonic waves (frequency  $< 0.5/T_p$ ). (d) Biphasic phase for the triad-interaction between incident subharmonic waves and short wave groups. (e) Measured time-averaged Eulerian velocity induced by subharmonic waves  $\tilde{u}$  between the maximum (crest,  $z = \eta_c$ ) and minimum (trough,  $z = \eta_t$ ) surface elevation level.

### 2.4.3. Subharmonic wave-induced mass transport

Figure 6 shows the mass transport  $\bar{M}^{(4)}$  (2.43) evaluated in the shoaling zone using measured and theoretical velocity statistics ( $\overline{\tilde{u}^2}$  and  $\tilde{u}[u^{(1)}|_{z=0}]^2$ ). As mentioned above, the experiment did not actually measure  $\bar{M}^{(4)}$  and thus does not allow comparison with (2.43). The comparison in figure 6 is essentially between the experimental and theoretical subharmonic velocity instead of  $\bar{M}^{(4)}$ .

The theory agrees with the experiment very well for case A1. For cases A2 and A3 the theory slightly underestimated the magnitudes of both term I ('Stokes drift' effect) and term II (skewness effect), indicating an underestimation of subharmonic velocity magnitude. Nevertheless, the theory aligns with experimental results regarding total transport, primarily due to the opposite signs of the two terms that cancel out the underestimations.

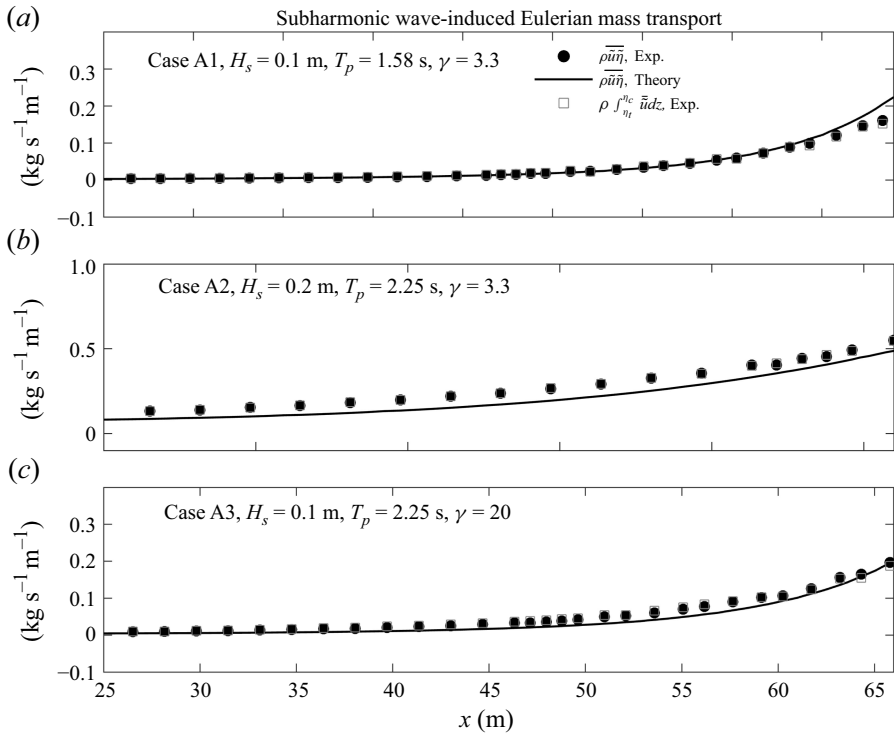


Figure 5. Subharmonic wave-induced mass transport components  $\rho\tilde{u}\tilde{\eta}$  and  $\rho \int_{\eta_t}^{\eta_c} \tilde{u} dz$  in the shoaling zone for (a) A1, (b) A2 and (c) A3 irregular wave cases of GLOBEX experiment. Dots: experiment; lines: theoretical predictions. Here,  $\rho = 1000(\text{kg m}^{-3})$  was adopted.

Term I contributes to a forward drift as it is proportional to the energy of the subharmonic velocity, whereas Term II accounts for a backward drift because the near anti-phase coupling between subharmonic wave and wave group results in a negative  $\tilde{u}[u^{(1)}]^2$ . In all three cases as depth decreases towards the shore the total transport is initially negative (seaward) and turns positive (shoreward) near the end of the shoaling zone due to the positive Term I growing faster than the negative Term II and becoming predominant prior to wave breaking. The results also suggest that the transition of total transport occurs at shallower relative depth  $k_p h$  for larger wave period and smaller bandwidth.

The measured Eulerian mass transports (crosses) in all three cases were lower than term I (red dots) alone but greater than the total transport (black dots), especially for a smaller period (figure 6a) and greater depth. This aligns with (2.41) that  $\tilde{u}\tilde{\eta}$  (the subscript of  $\tilde{u}_0$  for  $z = 0$  omitted since subharmonic waves are in shallow water in this case) accounts for the entire Term I contribution but only a fraction of the Term II contribution that is generally negative. It also stresses the necessity to include those negative velocity skewness contributions not accounted for by  $\tilde{u}\tilde{\eta}$  to correct its overprediction.

### 3. Numerical model of subharmonic wave-induced mass transport

#### 3.1. Non-hydrostatic wave model SWASH

To validate the theoretical model for subharmonic wave-induced mass transport, a Lagrangian particle-tracking simulation is conducted, which requires a high-resolution

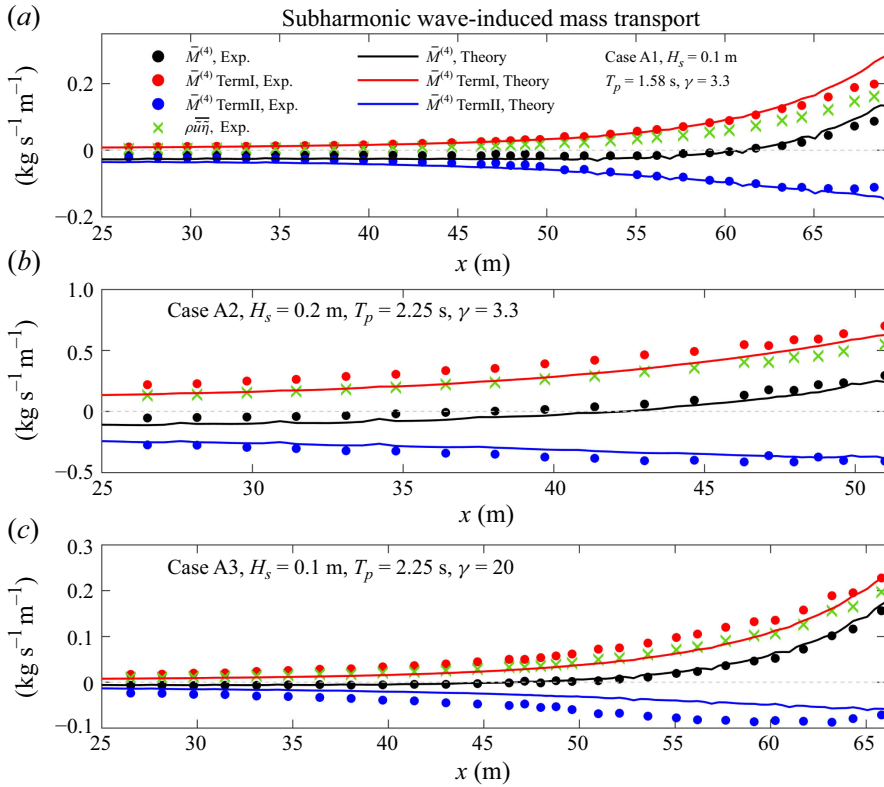


Figure 6. Subharmonic wave-induced mass transport  $\bar{M}^{(4)}$  (2.43) in the shoaling zone for (a) A1, (b) A2 and (c) A3 irregular wave cases of GLOBEX experiment. Dots: experiment; lines: theoretical predictions. Red and blue markers and lines denote the Term I ('Stokes drift' effect) and Term II (skewness effect) components in (2.43), respectively. Green crosses denote the same result as the dots in figure 5, i.e. the component  $\bar{u} \bar{\eta}$ . Here,  $\rho = 1000 \text{ (kg m}^{-3}\text{)}$  was adopted.

flow field in space and time not available from the experiment. Thus, the non-hydrostatic wave model SWASH (Zijlema *et al.* 2011) was used to investigate the subharmonic-induced mass transport for bichromatic wave groups propagating over a plane sloping ramp. The multilayer non-hydrostatic model SWASH is essentially a RANS (Reynolds-Averaged Navier–Stokes) solver without VOF (Volume Of Fluid) and level set type of free-surface capturing scheme, capable of resolving strong nonlinear wave motion. It solves the momentum and mass conservation equations

$$\frac{\partial u}{\partial t} + \frac{\partial uu}{\partial x} + \frac{\partial wu}{\partial z} = -\frac{1}{\rho} \frac{\partial (p_h + p_{nh})}{\partial x} + \frac{\partial \tau_{xz}}{\partial z} + \frac{\partial \tau_{xx}}{\partial x}, \quad (3.1)$$

$$\frac{\partial w}{\partial t} + \frac{\partial uw}{\partial x} + \frac{\partial ww}{\partial z} = -\frac{1}{\rho} \frac{\partial p_{nh}}{\partial z} + \frac{\partial \tau_{zz}}{\partial z} + \frac{\partial \tau_{zx}}{\partial x}, \quad (3.2)$$

$$\frac{\partial u}{\partial x} + \frac{\partial w}{\partial z} = 0, \quad (3.3)$$

where  $p_h$  is the hydrostatic pressure,  $p_{nh}$  is the non-hydrostatic pressure and  $\tau$  is the turbulent stress described by the standard  $K$ - $\epsilon$  model, where  $K$  is the turbulent kinetic energy and  $\epsilon$  is its dissipation rate in the present work. The model has been

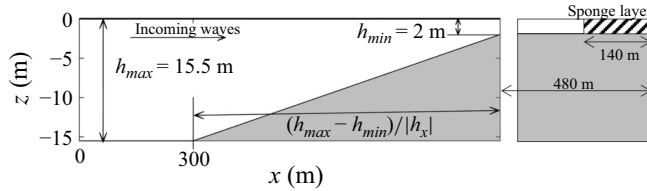


Figure 7. Schematic configuration of numerical flume set-up used for the SWASH model;  $h_x = dh/dx$  is the bottom slope.

$h_{max}$ [m]	$h_{min}$ [m]	$-h_x^{-1}$	$a_1$ [m]	$\omega_1$ [rad·s <sup>-1</sup> ]	$a_2$ [m]	$\omega_2$ [rad·s <sup>-1</sup> ]	$ \beta  =  h_x /k_g h$	$\mu = 1 - (c_g^2/gh)$
15.5	2	30/60/90/120	0.27	0.9676	0.09	0.7917	0.020~0.388	0.147~0.711

Table 1. Bathymetry parameters and bichromatic wave conditions for SWASH model.

extensively validated against both laboratory (de Bakker, Tissier & Ruessink 2016b) and field data (Rijnsdorp, Ruessink & Zijlema 2015) of the nearshore nonlinear evolution of subharmonic waves. Detailed descriptions of the model can be found in Rijnsdorp, Smit & Zijlema (2014) and Smit *et al.* (2014).

### 3.1.1. Model set-up and data processing

The numerical flume has a bed profile of a plane sloping ramp with bottom slope ranging between 1/30 and 1/120 connected with two flat bottom plateaux (figure 7). The toe of the ramp is 300 m away from the incident boundary and the plateau at the shallow end is 480 m long equipped with a 140 m sponge layer near the outgoing boundary to minimise reflection of short waves. The depth at the shallow end was carefully chosen to prevent wave breaking, thereby no surf zone occurs in the model domain. Eight sigma layers with thicknesses 6.06, 7.27, 8.73, 10.47, 12.57, 15.08, 18.10, 21.71 per cent of full depth were adopted. The bottom boundary layer and the associated mass transport caused by boundary layer streaming was not considered in the numerical model by adopting a zero bottom friction factor. The bathymetry and wave condition parameters are summarised in table 1.

Preliminary analysis of incoming and outgoing subharmonic waves using the same method as in § 2.4 indicated that the reflection is less than 5% for the subharmonic wave amplitude. The following analysis is based on the result before decomposition into incoming/outgoing components as there is no fundamental difference.

The SWASH model outputs the horizontal velocities at the centre of each vertical layer, where the absolute  $z$ -coordinate varies in time with the undulating surface elevation. To derive the Eulerian velocity at fixed heights, the velocity output at a time-dependent height was first vertically mapped onto fixed heights, including ten equidistant layers between the wave crest  $z = \eta_t$  and wave trough  $z = \eta_c$  and eight sigma layers between the bottom  $z = -h$  and wave trough  $z = \eta_t$ , using spline interpolation.

The horizontal Eulerian velocity  $u$  and surface elevation  $\eta$  were first demeaned and then low-pass filtered with cutoff frequency of  $0.5\omega$ , where  $\omega = (\omega_1 + \omega_2)/2$  is the central frequency of bichromatic waves, to obtain the surface elevation  $\tilde{\eta}$  and Eulerian velocity  $\tilde{u}$  of the subharmonic wave. The first-order velocity  $u^{(1)}$  was obtained by filtering through the band  $[0.5\omega, 1.5\omega]$ .

To make best use of the vertical distribution of velocity resolved by SWASH, the following relationship:

$$\frac{\cosh \left[ \frac{2k_p(z+h)}{\cosh^2 k_p h} \right]}{\cosh^2 k_p h} \left[ u^{(1)} \Big|_{z=0} \right]^2 = [1 + \tanh^2 k_p(z+h)] [u^{(1)}]^2, \quad (3.4)$$

is used to change (2.64) into an alternative form

$$\overline{u_L^{(4)}} = \frac{\overline{\tilde{u}^2}}{c_g} + \zeta \left( k_p h, \frac{z}{h} \right) [1 + \tanh^2 k_p(z+h)] \frac{[\overline{u^{(1)}}]^2 \tilde{u}}{cc_g}. \quad (3.5)$$

Equation (3.5) is evaluated both theoretically and numerically for comparison with the result from the Lagrangian particle-tracking simulation. The numerical evaluation calculates  $\overline{\tilde{u}^2}$  and  $[\overline{u^{(1)}}]^2 \tilde{u}$  first and then substitutes them into (3.5). The theoretical evaluation calculates  $\overline{\tilde{u}^2}$  and  $[\overline{u^{(1)}}]^2 \tilde{u}$  as

$$\overline{\tilde{u}^2} = \frac{1}{2} |\hat{u}_l|^2, \quad [\overline{u^{(1)}}]^2 \tilde{u} = \frac{1}{\sqrt{2}} \text{std}\{\widetilde{[u^{(1)}]^2}\} |\hat{u}_l| \cos \phi, \quad (3.6)$$

where  $|\hat{u}_l| \cos \phi$  ( $\phi = \text{biphase}$ ) is theoretically predicted from (2.27) while  $\text{std}\{\widetilde{[u^{(1)}]^2}\}$  (i.e. the standard deviation of low-pass filtered  $[u^{(1)}]^2$  in time dimension) is calculated from simulated  $u^{(1)}$ .

### 3.1.2. Lagrangian particle tracking and subharmonic wave-induced mass transport velocity

The Lagrangian particle tracking was conducted using the velocity field by the SWASH model. Let  $x_L(t)$  and  $z_L(t)$  be the horizontal and vertical coordinates of a tagged particle,  $u_L(t)$  and  $w_L(t)$  be the horizontal and vertical velocities, the particle displacement in one time step from  $t$  to  $t + \Delta t$  was given by

$$\begin{cases} x_L(t + \Delta t) - x_L(t) = u_L(t) \Delta t, \\ z_L(t + \Delta t) - z_L(t) = w_L(t) \Delta t, \end{cases} \quad (3.7)$$

where the velocities  $u_L(t)$  and  $w_L(t)$  were interpolated from the simultaneous SWASH flow field to the particle location  $x_L(t)$  and  $z_L(t)$  using the square inverse distance weighted interpolation (Shepard 1968).

To derive the mass transport velocity at a given location  $(x, z)$ , a particle is released from  $(x, z)$  and tracked for one wave group cycle of 35.72 s. This procedure is repeated 40 times with the release timepoint being increased by 1/20 wave group period successively to establish an ensemble average. A linear regression with respect to the tracking time  $t$  is applied to the resultant 40 records of  $x_L(t)$  to obtain the mass transport velocity at  $(x, z)$ .

## 3.2. Model results

### 3.2.1. Trajectories of Lagrangian particles

Figure 8(a) shows the numerical results of time-averaged total horizontal Eulerian velocity profiles over a 1/120 bed slope. Similar to the illustration in figure 1, the velocity is positive between the wave trough and crest, leading to a forward mass transport. Below the wave trough, a return current is formed and offsets the forward mass transport, resulting in a zero net mass transport in the numerical flume. The return current is skewed towards the surface and becomes more uniform vertically as the water depth decreases.

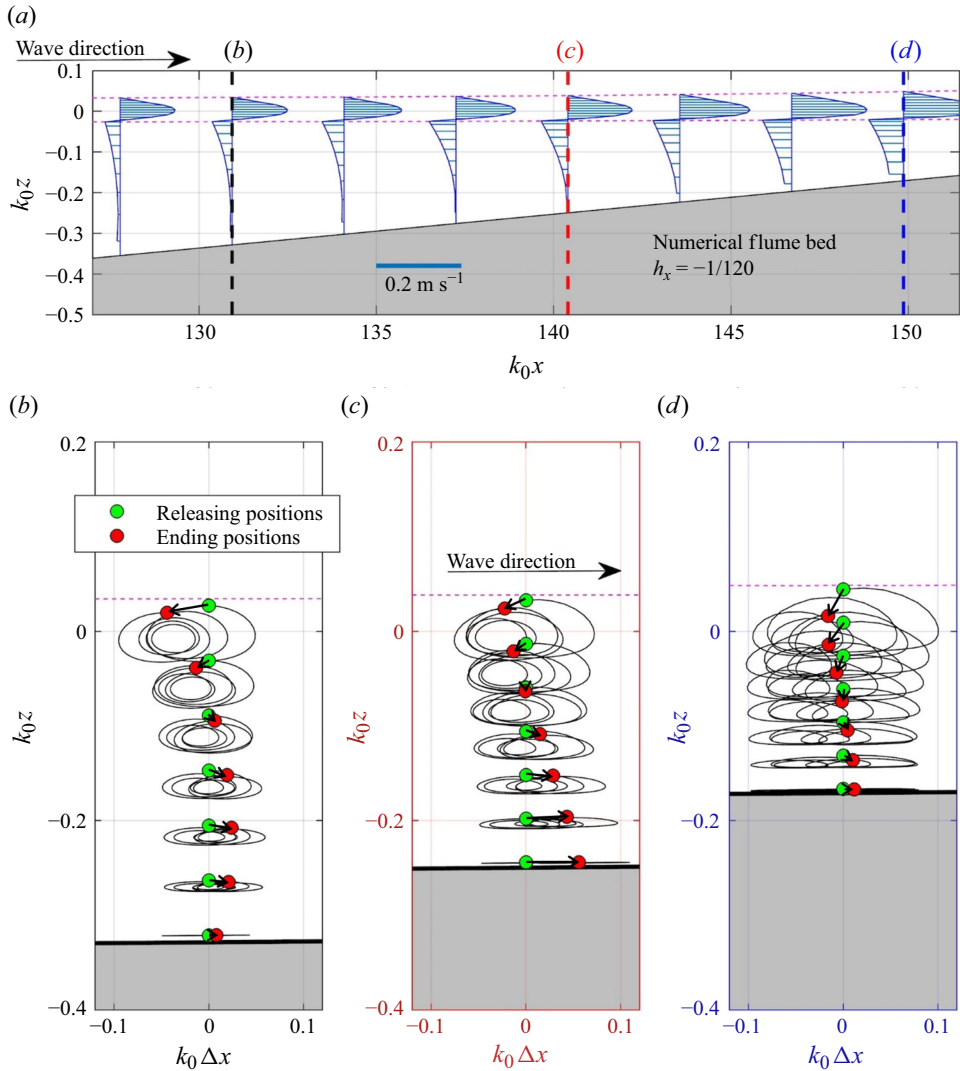


Figure 8. (a) Time-averaged total Eulerian horizontal velocity for the  $h_x = -1/120$  case simulated by the SWASH model. (b)–(d) Trajectories of fluid particles initially released at the timepoint of wave crest along the vertical profile of local depths (b)  $k_0 h = 0.33$ , (c)  $k_0 h = 0.25$  and (d)  $k_0 h = 0.17$  and tracked for one wave group cycle. The magenta dashed lines in (a) denote the wave crest and trough heights. Here,  $k_0 = \omega^2/g$  is the deep-water wavenumber. Green and red circles denote the starting and ending positions of the tagged particles, respectively.

Figure 8(b–d) shows the trajectories of particles released at various heights for three water depths shown in figure 8(a). Each particle was tracked over one wave group cycle, after which the particles near the surface moved backward while those near the bottom moved forward. This phenomenon results from the stronger return Eulerian current near the surface, as shown in figure 8(a), overpowering the forward Stokes drift near the surface, while the opposite is true near the bottom. At greater depths (figure 8b), a small proportion of particles near the surface moved backward while, as depth decreases, more particles moved backwards as the return current becomes more uniformly distributed in shallow water (figure 8d). Figure 8 also shows that particles move downward after a wave group

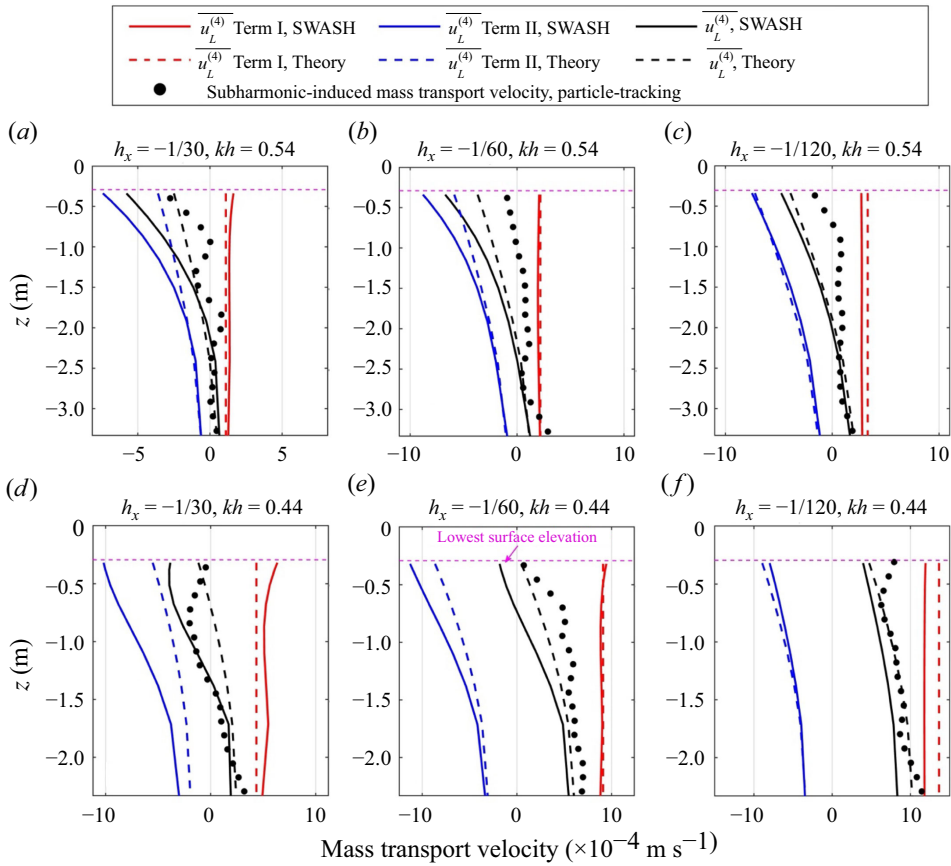


Figure 9. Profiles of mass transport velocity induced by subharmonic wave forced by bichromatic wave groups with amplitudes  $[a_1, a_2] = [0.27, 0.09]$  m and radian frequencies  $[\omega_1, \omega_2] = [0.9676, 0.7917]$  rad s<sup>-1</sup> over bottom slopes of 1/30 (a, d), 1/60 (b, e) and 1/120 (c, f). Upper:  $kh = 0.54$ ; lower:  $kh = 0.44$ . Black dots: difference between the mass transport velocity evaluated using Lagrangian particle-tracking model driven by SWASH flow field (cf. § 3.1.2) with and without the subharmonic velocity. Black, red and blue lines denote the subharmonic wave-induced mass transport velocity  $\overline{u_L^{(4)}}$ , the Term I ('Stokes drift' effect), and Term II (skewness effect) components predicted by (3.5). Equation (3.5) was evaluated using both simulated velocity (SWASH, solid lines) and theoretical subharmonic velocity (theory, dashed lines).

cycle, more so at a shallow depth (figure 8d) than at a deeper depth (figure 8b). Near the bed, however, particles no longer move downward and can only move forward along the bed.

### 3.2.2. Validation of subharmonic wave-induced mass transport solution

Figure 9 compares the profile of the subharmonic wave-induced mass transport velocity obtained by using Lagrangian particle tracking (dots), the value of  $\overline{u_L^{(4)}}$  by (3.5) evaluated numerically (SWASH, solid lines) and theoretically (theory, dashed lines). Both predictions using numerical and theoretical velocities agree well with the particle-tracking results, validating the theoretical model of subharmonic wave-induced mass transport.

The total mass transport velocity is positive at the bottom and decreases upwards, approaching zero or even a negative value towards the surface. This is well captured by the theoretical profile of  $\overline{u_L^{(4)}}$ , especially when evaluated using the simulated profile

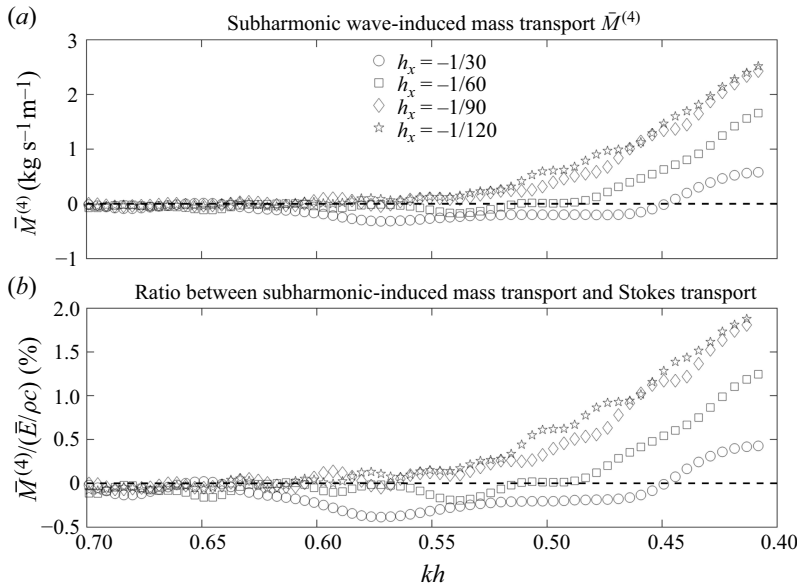


Figure 10. (a) Subharmonic wave induced mass transport  $\bar{M}^{(4)}$  (40) evaluated with SWASH-simulated velocity. (b) Percentage ratio between  $\bar{M}^{(4)}$  and Stokes transport  $\bar{E}/c$ . Here,  $\rho = 1000 \text{ (kg m}^{-3}\text{)}$  was adopted.

of  $[\overline{u^{(1)}}]^2 \tilde{u}$ . The theoretical profiles indicate that this is due to the greater negative Term II near the surface whereas profiles of Term I were almost vertically uniform, aligning with the theoretical assumption of shallow water for a subharmonic wave. Term I increases significantly in magnitude with decreasing bed slope and depth while Term II does not, resulting in the enhanced dominance of Term I over Term II over a mild slope and in shallow water, consistent with figure 3(b). Over the 1/30 bed slope at  $kh = 0.44$  (figure 9d), Term I marginally surpasses Term II while the advantage becomes apparent for 1/60 bed slope and (figure 9e). As the bed slope decreases to 1/120, Term I increases significantly while Term II does not, making Term I predominant and hence close to the total velocity (figure 9f).

### 3.2.3. Influences of bed slope on subharmonic wave-induced mass transport

Figure 10(a) presents the numerical results of  $\bar{M}^{(4)}$  (2.43) for bed slopes 1/30–1/120, showing that the mass transport increases with decreasing depth at a greater rate for gentler bed slopes. However, as the bed slope decreases from 1/90 to 1/120, the increase in mass transport becomes marginal. For bed slopes 1/30 and 1/60, the transport is negative (seaward) at deeper depths while it is positive near the end of the shoaling zone, consistent with the results derived from experimental data (figure 6). The results also indicate that, when the bed slope is not too mild (seemingly greater than 1/90 in this case), the transition from negative to positive transport occurs at deeper depths for milder bed slopes, which also aligns with figure 2(b).

The percentage ratio of  $\bar{M}^{(4)}$  to the Stokes transport of short waves  $\bar{E}/c$  (figure 10b) shows a similar trend to  $\bar{M}^{(4)}$  in figure 10(a), indicating little effect of the bed slope on the Stokes transport. Specifically, as the bed slope decreases from 1/30 to 1/90, the maximum subharmonic wave-induced mass transport at the shallow-water end increased from approximately 0.5 % to 2 % of the Stokes transport but remained almost unchanged

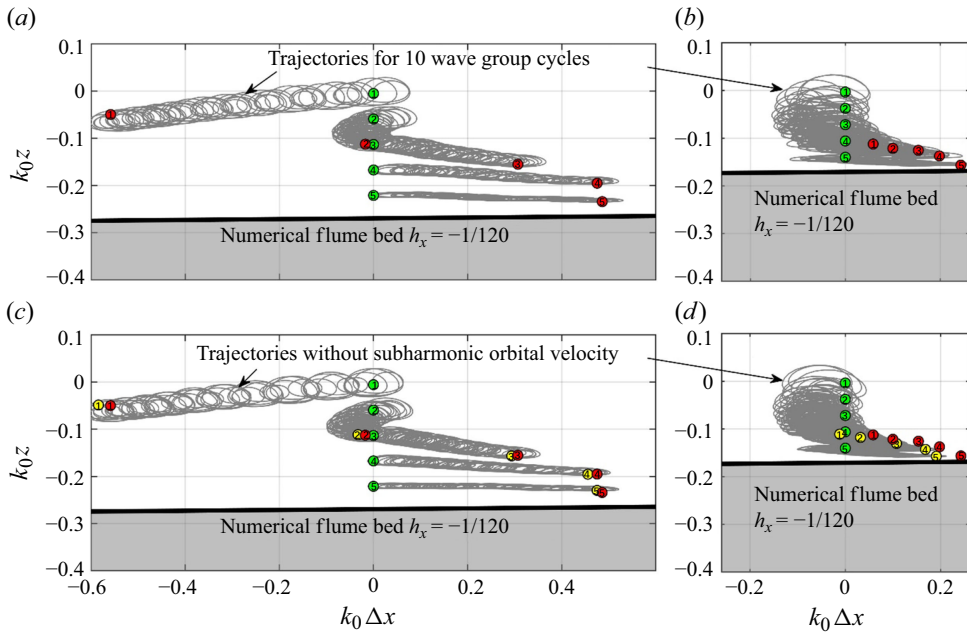


Figure 11. Fluid particle trajectories over ten wave group cycles (fifty wave cycles). Upper: particles driven by flow field simulated by SWASH model initially released at 5 different heights at water depth (a)  $k_0 h = 0.27$  and (b)  $k_0 h = 0.17$ ; lower: particles driven by flow field after removing the subharmonic orbital velocity. Releasing profiles in (c) and (d) are same as in (a) and (b), respectively. The red circles in (c)–(d) are duplicates of those in (a)–(b) for comparison.  $k_0 = \omega^2/g$  is the deep-water wavenumber. Here,  $\Delta x$  denotes the horizontal displacement of particles. Green and red/yellow circles denote the starting and ending position of the tagged particles with/without subharmonic orbital velocity, respectively.

as the bed slope decreases further from  $1/90$  to  $1/120$ . It is also noticed that for bed slope  $1/30$  the negative  $\bar{M}^{(4)}$  around  $kh = 0.57$  is nearly  $0.5\%$  of the Stokes transport, which is comparable to the ratio of the maximum  $\bar{M}^{(4)}$  to the Stokes transport at the end of shoaling zone. Although the ratio between  $\bar{M}^{(4)}$  and the Stokes transport is generally low, below  $2\%$ , according to (2.13) and (2.26),  $\tilde{u}$  generally scales with  $\tilde{E}/(hc)$ , thus this ratio relates to the short wave amplitude approximately as

$$\frac{\bar{M}^{(4)}}{\bar{E}/c} \propto \frac{\left(\frac{\tilde{E}}{hc}\right)^2 \frac{h}{c_g}}{\bar{E}/c} \sim \frac{(a_1 a_2 / h)^2}{a_1^2 + a_2^2} = \left(\frac{h^2}{a_1^2} + \frac{h^2}{a_2^2}\right)^{-1}, \quad (3.8)$$

therefore, higher relative importance of  $\bar{M}^{(4)}$  is expected for larger waves. This is natural since  $\bar{M}^{(4)}$  scales with  $a^4$  while  $\bar{E}$  scales with  $a^2$ . More results are needed to exam this relationship.

### 3.2.4. Long-term effect of subharmonic wave-induced mass transport

Despite being secondary to Stokes transport of short waves, the effect of subharmonic wave-induced mass transport on particle movements accumulates with time and travel distance and becomes important in the long term. Figure 11(a–b) illustrates the trajectories of particles across 10 wave group cycles released at 5 heights at two water depths over a  $1/120$  bed slope. At the greater depth in figure 11(a), the particle movement maintained a

similar trend as that over one wave group cycle (figure 8c). At a shallow depth (figure 11b), the particle movement near the bed maintained a similar trend along the bed as depicted in figure 8(d), while those released near the surface initially moved backward after one wave group cycle (figure 8d) but eventually moved forward after ten wave group cycles. This is due to the marked downward movement of particles initially near the surface (figure 8d), ultimately aligning them with the forward-moving trajectories of particles in the middle and lower water column.

Figure 11(c,d) demonstrates the same results as (figure 11a,b) but without the subharmonic velocity. A comparison between figure 11(a) and c and the difference between the red and yellow circles in figure 11(c,d) reveal that the subharmonic orbital motion induces a weak net forward drift. This forward drift becomes more significant at shallow depths (figures 11b and 11d) especially for those released near the surface that drifted slowly at the leading order, which by contrast highlights the importance of the contribution of subharmonic wave-induced drift.

#### 4. Conclusion and discussion

This study develops and validates a theoretical solution for the first time for mass transport as well as the associated drift velocity induced by group-forced subharmonic (infragravity) waves over an undulating bottom topography. The fourth-order solution for Lagrangian mass transport velocity incorporates the kinematic effects driven by both the subharmonic wave-induced velocity variance and skewness. The theory was validated by GLOBEX experiment and Lagrangian particle-tracking simulations driven by the SWASH model. Additionally, the analytical solution was applied to the experimental data from the GLOBEX campaign to demonstrate its applicability under field conditions.

The theory identifies two key kinematic mechanisms contributing to subharmonic wave-induced mass transport: (i) a forward drift analogous to Stokes drift, arising from the self-interaction of subharmonic orbital motion that is proportional to the variance (energy) of the subharmonic velocity, and (ii) a depth-decaying backward drift arising from the negative velocity skewness induced by the near anti-phase coupling between subharmonic waves and short wave groups. For relative bed slope  $|\beta|$  less than  $\sim 0.01$ , these two mechanisms are comparable at around  $kh \approx 0.72$ , and this critical value decreases with increasing bed slope, wave period and decreasing bandwidth. In deeper water or over steeper bed slopes, the backward drift can exceed the forward drift near the surface, producing a net seaward transport in the upper water column. As water depth decreases, forward drift increases and dominates net positive mass transport, especially over mild slopes.

Although subharmonic-induced transport is typically smaller than the classical Stokes transport (e.g. reaching up to  $\sim 2\%$  of Stokes transport at  $kh \approx 0.42$  over a  $1/120$  slope), its influence on material transport accumulates over time and distance and is vertically distributed across the entire water column. These characteristics, therefore, make subharmonic-induced transport particularly relevant in shallow coastal regions, especially where Stokes drift is nearly cancelled by the Eulerian return flow, leaving subharmonic contributions the key driver of particle motion. Based on the expression of mass transport obtained, it is evident that the relative importance of subharmonic-induced transport to Stokes transport increases with short wave amplitude.

The subharmonic wave-induced mass transport provides the new third mechanism for sediment transport. Despite the skewness-induced sediment transport (Deigaard *et al.* 1999; Yu, Hsu & Hanes 2010; Baldock *et al.* 2011) arising from group-modulated sediment concentration near the bottom, however, the present skewness-induced mass transport

is a purely kinematic effect of subharmonic wave motion so that it affects the whole water column from surface to bottom, therefore, influences the movement of non-inertial particles at the wave surface (e.g. buoyant microplastics). The latter was previously thought to be affected solely by Stokes drift from short waves.

**Acknowledgements.** We thank Q. Liu from Tianjin University for checking the calculation of fourth-order Lagrangian velocity in the shallow-water limit. We are grateful to the anonymous reviewers whose input greatly improved the manuscript.

**Funding.** Z.L. and Q.Z. have been supported by the Natural Environment Research Council of the UK (Grant No. NE/V006088/1).

**Declaration of interests.** The authors report no conflict of interest.

## Appendix A. Subharmonic wave-induced mass transport in Eulerian system

1. Broad-banded waves with  $\alpha = O(1)$  then

$$k_{m,n}h = O(\alpha k_m h) = O(k_m h). \quad (\text{A1})$$

1.1. Deep water  $|k_{m,n}|h = O(k_m h) \gg 1$

In this case  $\tanh k_{m,n}h = \text{sign}(k_{m,n})[1 + O(e^{-k_m h})] = \text{sign}(\omega_{m,n})[1 + O(e^{-k_m h})]$ , equation (2.39) becomes

$$\bar{M}^{(4)} = \sum_{m,n} \frac{1}{2} \frac{\hat{U}_{m,n} \hat{U}_{m,n}^*}{|\omega_{m,n}|} + \frac{\max(k_m \omega_m, k_n \omega_n)}{\omega_m \omega_n |\omega_{m,n}|} \hat{u}_m^* \hat{u}_n \hat{U}_{m,n}, \quad (\text{A2})$$

with an error factor  $1 + O(e^{-k_m h})$ .

Invoking the deep-water dispersion relationship

$$k_m = \frac{\omega_m^2}{g} [1 + O(e^{-2k_m h})], \quad (\text{A3})$$

equation (A2) reduces to

$$\bar{M}^{(4)} = \sum_{m,n} \frac{1}{2} \frac{\hat{U}_{m,n} \hat{U}_{m,n}^*}{|\omega_{m,n}|} + \frac{\max(\omega_m^3, \omega_n^3)}{\omega_m \omega_n |\omega_{m,n}|} \frac{\hat{u}_m^* \hat{u}_n \hat{U}_{m,n}}{g}, \quad (\text{A4})$$

with an error factor  $[1 + O(e^{-2k_m h})]$ .

1.2. Intermediate depth  $|k_{m,n}|h = O(k_m h) = O(1)$

In this case the generalised solution (2.39) must be invoked.

1.3. Shallow water  $|k_{m,n}|h = O(k_m h) \ll 1$

In this case, the dispersion relationship becomes

$$\frac{\omega_m}{k_m} = \frac{\omega_n}{k_n} = \frac{\omega_{m,n}}{k_{m,n}} = \sqrt{gh} [1 + O(k_m^2 h^2)], \quad (\text{A5})$$

and (2.39) reduces to

$$\bar{M}^{(4)} = \sqrt{\frac{h}{g}} \sum_{m,n} \frac{1}{2} \hat{U}_{m,n} \hat{U}_{m,n}^* + \frac{3}{g} \sum_{m,n} \frac{1}{2} \hat{u}_m^* \hat{u}_n \hat{U}_{m,n}, \quad (\text{A6})$$

with an error factor  $1 + O(k_m^2 h^2)$ .

Furthermore, recall  $\tilde{u}$  and  $u^{(1)}$  in (2.33) and (2.4), respectively, we have the relationships

$$\overline{\tilde{u}^2}\Big|_{z=0} = \overline{Re \left[ \sum_{m,n} \hat{U}_{m,n} e^{i\theta_{m,n}} \right] Re \left[ \sum_{m,n} \hat{U}_{m,n} e^{i\theta_{m,n}} \right]} = \frac{1}{2} \sum_{m,n} \hat{U}_{m,n} \hat{U}_{m,n}^*, \quad (\text{A7})$$

$$\overline{\tilde{u} [u^{(1)}]^2}\Big|_{z=0} = \overline{Re \left[ \sum_m \hat{u}_m e^{i\theta_m} \right] Re \left[ \sum_n \hat{u}_n e^{i\theta_n} \right] Re \left[ \sum_{m,n} \hat{U}_{m,n} e^{i\theta_{m,n}} \right]} = \frac{1}{2} \sum_{m,n} \hat{u}_m^* \hat{u}_n \hat{U}_{m,n}. \quad (\text{A8})$$

And therefore (A6) can be recovered in the time domain as

$$\bar{M}^{(4)} = \sqrt{\frac{h}{g} \overline{\tilde{u}^2}} + \frac{3}{g} \overline{[u^{(1)}]^2} \tilde{u}, \quad (\text{A9})$$

where the velocities at arbitrary depth instead of at  $z = 0$  are used with the same error factor  $1 + O(k_m^2 h^2)$ .

2. Narrow-banded waves with  $\alpha \ll 1$  with central frequency/wavenumber  $\omega_p/k_p$  then

$$|k_{m,n}| h = O(\alpha k_m h) = O(\alpha k_p h) \ll O(k_p h). \quad (\text{A10})$$

2.1. Deep water for both short and subharmonic waves  $1 \ll |k_{m,n}| h \ll O(k_p h)$

In this case, equation (A4) applies but with the coefficient of the second term approximated as

$$\frac{\max(\omega_m^3, \omega_n^3)}{\omega_m \omega_n |\omega_{m,n}|} = \frac{\omega_p}{|\omega_{m,n}|} [1 + O(\alpha)], \quad (\text{A11})$$

hence it becomes

$$\bar{M}^{(4)} = \sum_{m,n} \frac{1}{2} \frac{\hat{U}_{m,n} \hat{U}_{m,n}^*}{|\omega_{m,n}|} + \frac{\omega_p}{|\omega_{m,n}|} \frac{\hat{u}_m^* \hat{u}_n \hat{U}_{m,n}}{g} \quad (\text{A12})$$

with an error factor  $1 + O(\alpha, e^{-2|k_{m,n}|h})$ .

2.2. Deep water for short wave, intermediate depth for subharmonic waves  $|k_{m,n}| h = O(1) \ll O(k_p h)$

Let  $(k_m h, k_n h) = O(k_p h) \gg 1$  but keep  $k_{m,n} h = O(1)$  and invoke the deep-water dispersion relationship (A3), equation (2.39) becomes approximately

$$\bar{M}^{(4)} = \sum_{m,n} \hat{U}_{m,n} \hat{U}_{m,n}^* \frac{\tanh k_{m,n} h}{2\omega_{m,n}} + \frac{\omega_p \tanh k_{m,n} h}{\omega_{m,n}} \frac{\hat{u}_m^* \hat{u}_n \hat{U}_{m,n}}{g}, \quad (\text{A13})$$

with an error factor  $1 + O(\alpha, k_p^{-1} h^{-1})$  for the second term.

### 2.3. Deep water for short wave, shallow water for subharmonic waves $|k_{m,n}|h \ll 1 \ll O(k_ph)$

Let  $|k_{m,n}|h \ll 1$  in (2.39), it becomes

$$\bar{M}^{(4)} = \sum_{m,n} \hat{U}_{m,n} \hat{U}_{m,n}^* \frac{k_{m,n}h}{2\omega_{m,n}} + \frac{\omega_p k_{m,n}h}{\omega_{m,n}} \frac{\hat{u}_m^* \hat{u}_n \hat{U}_{m,n}}{g}, \quad (\text{A14})$$

with an error factor  $1 + O(k_{m,n}^3 h^3)$ . For narrow-banded waves introduce the approximation

$$\begin{cases} k_n = \frac{\omega_p}{c} + \frac{\omega_n - \omega_p}{c_g} + O[(\omega_n - \omega_p)^2] \\ k_m = \frac{\omega_p}{c} + \frac{\omega_m - \omega_p}{c_g} + O[(\omega_m - \omega_p)^2] \end{cases} \quad (\text{A15})$$

where

$$c = \frac{\omega_p}{k_p} = \frac{g}{\omega_p} [1 + O(e^{-k_ph})], \quad c_g = \left. \frac{\partial \omega}{\partial k} \right|_{\omega=\omega_p} = \frac{g}{2\omega_p} [1 + O(e^{-k_ph})], \quad (\text{A16})$$

are the deep-water wave phase and group speed corresponding to central frequency  $\omega_p$ , respectively. The coefficient of Term I in (A14) is thus approximately

$$\frac{k_{m,n}}{\omega_{m,n}} = \frac{1}{c_g} [1 + O(\alpha)] = \frac{2\omega_p}{g} [1 + O(\alpha, e^{-k_ph})]. \quad (\text{A17})$$

Therefore, (A14) reduces to

$$\bar{M}^{(4)} = \frac{\omega_p h}{g} \sum_{m,n} \hat{U}_{m,n} \hat{U}_{m,n}^* + \frac{2\omega_p^2 h}{g^2} \sum_{m,n} \hat{u}_m^* \hat{u}_n \hat{U}_{m,n}, \quad (\text{A18})$$

with an error factor  $1 + O(k_{m,n}^3 h^3, \alpha, e^{-2k_ph})$ .

Like (A6), (A18) can be recovered in time domain as

$$\bar{M}^{(4)} = \frac{2\omega_p}{g} \bar{u}^2 h + \frac{4\omega_p^2}{g^2} \left[ u^{(1)} \Big|_{z=0} \right]^2 \bar{u} h. \quad (\text{A19})$$

### 2.4. Intermediate depth for short waves, shallow water for subharmonic waves $|k_{m,n}|h \ll O(k_ph) = O(1)$

Let  $(k_m h, k_n h) = k_p h [1 + O(\alpha)] = O(1)$  and  $k_{m,n} h \ll O(1)$ , equation (2.39) becomes

$$\bar{M}^{(4)} = \frac{h}{2c_g} \sum_{m,n} \hat{U}_{m,n} \hat{U}_{m,n}^* + \left[ \left( \frac{1}{cc_g} + \frac{1}{c^2} \right) \frac{\tanh k_ph}{k_ph} + \frac{1 + \tanh^2 k_ph}{cc_g} \right] \sum_{m,n} \frac{\hat{u}_m^* \hat{u}_n \hat{U}_{m,n} h}{2}, \quad (\text{A20})$$

with an error factor  $[1 + O(k_{m,n}^2 h^2, \alpha)]$  and  $c$  and  $c_g$  take the general expressions

$$c = \frac{\omega_p}{k_p} = \sqrt{\frac{g \tanh k_ph}{k_p}}, \quad c_g = \left. \frac{\partial \omega}{\partial k} \right|_{\omega=\omega_p} = c \left( \frac{1}{2} + \frac{k_ph}{\sinh 2k_ph} \right). \quad (\text{A21})$$

Equation (A20) can be recovered in time domain as

$$\bar{M}^{(4)} = \frac{\bar{u}^2 h}{c_g} + \left( \frac{3 \tanh k_p h}{2 k_p h} + \frac{2 \cosh 2k_p h + 1}{2 \cosh^2 k_p h} \right) \frac{[u^{(1)}|_{z=0}]^2 \bar{u} h}{c c_g}. \quad (\text{A22})$$

And for  $k_p h \gg 1$  (A22) reduces to (A19).

## 2.5. Shallow water for both short and subharmonic waves $|k_{m,n}|h \ll O(k_p h) \ll 1$

In this case the result is given by equations (A6) and (A9), which can also be obtained for  $k_p h \ll 1$  in (A22).

## Appendix B. Proof of equivalence between $D_{m,n}$ in Eulerian and Lagrangian systems

The coefficient  $D_{m,n}$  obtained in Lagrangian system (2.63) writes as

$$\begin{aligned} D_{m,n} = & \left( \frac{1}{\omega_m} \frac{\tanh k_m h - \tanh k_{m,n} h}{h} + \frac{1}{\omega_n} \frac{\tanh k_n h + \tanh k_{m,n} h}{h} \right) \frac{k_{m,n}}{\omega_{m,n}} \\ & + \frac{k_m k_n}{\omega_m \omega_n} \left( \frac{\omega_m}{\omega_{m,n}} \frac{\tanh k_n h + \tanh k_{m,n} h}{k_m h} \right. \\ & \left. - \frac{\omega_n}{\omega_{m,n}} \frac{\tanh k_m h - \tanh k_{m,n} h}{k_n h} \right) \\ & + \frac{\omega_m k_m (\tanh k_n h + \tanh k_{m,n} h) - \omega_n k_n (\tanh k_m h - \tanh k_{m,n} h)}{\omega_m \omega_n \omega_{m,n} h} \\ & - \frac{2k_{m,n}^2 \tanh k_m h - \tanh k_n h}{\omega_m \omega_n k_{m,n} h}. \end{aligned} \quad (\text{B1})$$

Using the following relationship of the tanh function:

$$\tanh k_{m,n} h - \tanh k_m h + \tanh k_n h = \tanh k_{m,n} h \tanh k_m h \tanh k_n h, \quad (\text{B2})$$

the first term in (B1) may be rewritten as

$$\begin{aligned} & \left( \frac{1}{\omega_m} \frac{\tanh k_m h - \tanh k_{m,n} h}{h} + \frac{1}{\omega_n} \frac{\tanh k_n h + \tanh k_{m,n} h}{h} \right) \frac{k_{m,n}}{\omega_{m,n}} \\ & = \frac{k_{m,n}}{\omega_{m,n}} \left( \frac{k_m}{\omega_m} \frac{\tanh k_m h}{k_m h} + \frac{k_n}{\omega_n} \frac{\tanh k_n h}{k_n h} \right) + \frac{k_{m,n}^2 \tanh k_{m,n} h}{\omega_m \omega_n k_{m,n} h}. \end{aligned} \quad (\text{B3})$$

The second and third terms can be combined as

$$\begin{aligned} & \frac{k_m k_n}{\omega_m \omega_n} \left( \frac{\omega_m}{\omega_{m,n}} \frac{\tanh k_n h + \tanh k_{m,n} h}{k_m h} - \frac{\omega_n}{\omega_{m,n}} \frac{\tanh k_m h - \tanh k_{m,n} h}{k_n h} \right) \\ & + \frac{k_m k_n}{\omega_m \omega_n} \left( \frac{\omega_m}{\omega_{m,n}} \frac{\tanh k_n h + \tanh k_{m,n} h}{k_n h} - \frac{\omega_n}{\omega_{m,n}} \frac{\tanh k_m h - \tanh k_{m,n} h}{k_m h} \right) \\ & = \frac{k_m k_n}{\omega_m \omega_n} \left( \frac{\omega_m}{\omega_{m,n}} \frac{\tanh k_m h + \tanh k_{m,n} h \tanh k_m h \tanh k_n h}{k_m h} \right. \\ & \quad \left. - \frac{\omega_n}{\omega_{m,n}} \frac{\tanh k_m h - \tanh k_{m,n} h \tanh k_m h \tanh k_n h}{k_n h} \right) \end{aligned}$$

$$\begin{aligned}
 & - \frac{\omega_n}{\omega_{m,n}} \frac{\tanh k_n h - \tanh k_{m,n} h \tanh k_m h \tanh k_n h}{k_n h} \Big) \\
 & + \frac{k_m k_n}{\omega_m \omega_n} \left( \frac{\omega_m}{\omega_{m,n}} \frac{\tanh k_n h + \tanh k_{m,n} h}{k_n h} - \frac{\omega_n}{\omega_{m,n}} \frac{\tanh k_m h - \tanh k_{m,n} h}{k_m h} \right) \\
 & = \frac{k_m k_n}{\omega_m \omega_n} \left( \frac{\tanh k_m h}{k_m h} + \frac{\tanh k_n h}{k_n h} + \frac{\omega_m}{\omega_{m,n}} \frac{\tanh k_{m,n} h \tanh k_m h \tanh k_n h}{k_m h} \right. \\
 & \quad \left. + \frac{\omega_n}{\omega_{m,n}} \frac{\tanh k_{m,n} h \tanh k_m h \tanh k_n h}{k_n h} + \frac{\omega_m}{\omega_{m,n}} \frac{\tanh k_n h}{k_n h} + \frac{\omega_n}{\omega_{m,n}} \frac{\tanh k_m h}{k_m h} \right) \\
 & = \frac{k_m k_n}{\omega_m \omega_n} \left( \frac{\tanh k_m h}{k_m h} + \frac{\tanh k_n h}{k_n h} \right. \\
 & \quad \left. + \frac{1}{\omega_{m,n}} \frac{(\omega_n + \omega_{m,n}) \tanh k_{m,n} h \tanh k_m h \tanh k_n h + (\omega_m - \omega_{m,n}) \tanh k_{m,n} h}{k_m h} \right. \\
 & \quad \left. + \frac{1}{\omega_{m,n}} \frac{(\omega_m - \omega_{m,n}) \tanh k_{m,n} h \tanh k_m h \tanh k_n h + (\omega_n + \omega_{m,n}) \tanh k_{m,n} h}{k_n h} \right) \\
 & = \frac{k_m k_n}{\omega_m \omega_n} \left( \frac{\tanh k_m h}{k_m h} + \frac{\tanh k_n h}{k_n h} \right) + \left( \frac{\omega_m}{k_m} + \frac{\omega_n}{k_n} \right) \frac{k_{m,n}}{\omega_{m,n}} \frac{\tanh k_{m,n} h}{k_{m,n} h} \\
 & \quad + \left( \frac{\omega_n}{k_m} + \frac{\omega_m}{k_n} \right) \frac{k_{m,n}}{\omega_{m,n}} \frac{\tanh k_{m,n} h \tanh k_m h \tanh k_n h}{k_{m,n} h} + \frac{k_{m,n}^2}{k_m k_n} \frac{\tanh k_m h - \tanh k_n h}{k_{m,n} h}.
 \end{aligned} \tag{B4}$$

Substituting (B3) back into (B1) and using the relationship

$$\frac{k_{m,n}^2}{\omega_m \omega_n} \frac{\tanh k_{m,n} h}{k_{m,n} h} - \frac{k_{m,n}^2}{\omega_m \omega_n} \frac{\tanh k_m h - \tanh k_n h}{k_{m,n} h} = \frac{k_{m,n}^2}{\omega_m \omega_n} \frac{\tanh k_m h \tanh k_n h \tanh k_{m,n} h}{k_{m,n} h}, \tag{B5}$$

equation (B1) becomes

$$\begin{aligned}
 D_{m,n} & = \frac{k_{m,n}}{\omega_{m,n}} \left( \frac{\tanh k_m h}{\omega_m h} + \frac{\tanh k_n h}{\omega_n h} \right) + \frac{k_m k_n}{\omega_m \omega_n} \left( \frac{\tanh k_m h}{k_m h} + \frac{\tanh k_n h}{k_n h} \right) \\
 & \quad + \left( \frac{\omega_m}{k_m} + \frac{\omega_n}{k_n} \right) \frac{k_{m,n}}{\omega_{m,n}} \frac{\tanh k_{m,n} h}{k_{m,n} h} \\
 & \quad + \left[ \left( \frac{k_n}{\omega_m} + \frac{k_m}{\omega_n} \right) \frac{k_{m,n}}{\omega_{m,n}} + \frac{k_{m,n}^2}{\omega_m \omega_n} \right] \frac{\tanh k_m h \tanh k_n h \tanh k_{m,n} h}{k_{m,n} h},
 \end{aligned} \tag{B6}$$

which is same as that obtained in Eulerian system (2.40).

## Appendix C. Subharmonic wave-induced Lagrangian mass transport velocity

1. Broad-banded waves with  $\alpha = O(1)$  then

$$k_{m,n} h = O(\alpha k_m h) = O(k_m h). \tag{C1}$$

1.1. Deep water  $|k_{m,n}|h = O(k_m h) \gg 1$

In this case we have the following approximations:

$$\cosh [2k_m(z+h)] = \frac{1}{2}e^{2k_m(z+h)}[1 + O(e^{-4k_m h})], \quad (C2)$$

$$\cosh [2k_{m,n}(z+h)] = \frac{1}{2}e^{2|k_{m,n}|(z+h)}[1 + O(e^{-4k_m h})], \quad (C3)$$

$$\cosh^2 k_{m,n}h = \frac{1}{4}e^{2|k_{m,n}|h}[1 + O(e^{-2k_m h})], \quad (C4)$$

$$\cosh k_m h \cosh k_n h \cosh k_{m,n} h = \frac{1}{8}e^{2 \max(k_m, k_n)h}[1 + O(e^{-2k_m h})], \quad (C5)$$

and equation (2.61) becomes approximately

$$\begin{aligned} \overline{u_L^{(4)}} &= \sum_{m,n} \frac{k_{m,n}}{\omega_{m,n}} \widehat{U}_{m,n} \widehat{U}_{m,n}^* e^{2|k_{m,n}|z} \\ &\quad + \frac{k_{m,n} \max(\omega_m k_m, \omega_n k_n) + k_m k_n \max(\omega_m, \omega_n) + \max(\omega_m k_m^2, \omega_n k_n^2)}{\omega_m \omega_n | \omega_{m,n} |} \\ &\quad \times \widehat{u}_m^* \widehat{u}_n \widehat{U}_{m,n} e^{2 \max(k_m, k_n)z} \\ &= \sum_{m,n} \frac{k_{m,n}}{\omega_{m,n}} \widehat{U}_{m,n} \widehat{U}_{m,n}^* e^{2|k_{m,n}|z} + \frac{2 \max(k_m^2 \omega_m, k_n^2 \omega_n)}{\omega_m \omega_n | \omega_{m,n} |} \widehat{u}_m^* \widehat{u}_n \widehat{U}_{m,n} e^{2 \max(k_m, k_n)z}, \end{aligned} \quad (C6)$$

with an error factor  $1 + O(e^{-2k_m h})$ . Invoking the deep-water dispersion relationship (A3), equation (C6) becomes

$$\overline{u_L^{(4)}} = \sum_{m,n} \frac{\omega_m + \omega_n}{g} \widehat{U}_{m,n} \widehat{U}_{m,n}^* e^{\frac{2|\omega_m^2 - \omega_n^2|z}{g}} + \frac{2 \max(\omega_m^5, \omega_n^5)}{\omega_m \omega_n | \omega_{m,n} |} \frac{\widehat{u}_m^* \widehat{u}_n \widehat{U}_{m,n}}{g^2} e^{2 \max(\omega_m^2, \omega_n^2) \frac{z}{g}}, \quad (C7)$$

with an error factor  $[1 + O(e^{-2k_m h})]$ . Integrating (C7) from  $z = -\infty$  to  $z = 0$  recovers (A4).

### 1.2. Intermediate depth $|k_{m,n}|h = O(k_m h) = O(1)$

In this case the generalised solution (2.61) must be invoked.

### 1.3. Shallow water $|k_{m,n}|h = O(k_m h) \ll 1$

In this case we substitute the shallow-water dispersion relationship (A5)

$$\overline{u_L^{(4)}} = \frac{1}{\sqrt{gh}} \sum_{m,n} \widehat{U}_{m,n} \widehat{U}_{m,n}^* + \frac{3}{gh} \sum_{m,n} \widehat{u}_m^* \widehat{u}_n \widehat{U}_{m,n}, \quad (C8)$$

which can be recovered in time domain as

$$\overline{u_L^{(4)}} = \frac{\tilde{u}^2}{\sqrt{gh}} + \frac{3}{gh} [\overline{u^{(1)}}]^2 \tilde{u}. \quad (C9)$$

Multiplying (C9) with  $h$  yields (A9).

2. Narrow-banded waves with  $\alpha \ll 1$  then

$$|k_{m,n}|h = O(\alpha k_m h) = O(\alpha k_p h) \ll O(k_p h). \quad (\text{C10})$$

2.1. Deep water for both short and subharmonic waves  $1 \ll |k_{m,n}|h \ll O(k_p h)$

In this case equation (C7) applies but with  $\omega_m$  and  $\omega_n$  replaced by  $\omega_p[1 + O(\alpha)]$

$$\overline{u_L^{(4)}} = \sum_{m,n} \frac{2\omega_p}{g} \widehat{U}_{m,n} \widehat{U}_{m,n}^* e^{\frac{4\omega_p |\omega_{m,n}|}{g} z} + \frac{2\omega_p^3}{|\omega_{m,n}|} \frac{\widehat{u}_m^* \widehat{u}_n \widehat{U}_{m,n}}{g^2} e^{\frac{2\omega_p^2}{g} z}, \quad (\text{C11})$$

with an error factor  $[1 + O(\alpha, e^{-2|k_{m,n}|h})]$ . Integrating (C11) vertically from  $z = -\infty$  to  $z = 0$  recovers (A12).

2.2. Deep water for short wave, intermediate depth for subharmonic waves  $|k_{m,n}|h = O(1) \ll O(k_p h)$

Let  $(k_m h, k_n h) = O(k_p h) \gg 1$  but keep  $k_{m,n} h = O(1)$  and invoke the deep-water dispersion relationship (A3), then equation (2.61) becomes approximately

$$\overline{u_L^{(4)}} = \sum_{m,n} \frac{\omega_p}{g} \widehat{U}_{m,n} \widehat{U}_{m,n}^* \frac{\cosh[2k_{m,n}(z+h)]}{\cosh^2 k_{m,n} h} + \frac{2\omega_p^3 \tanh k_{m,n} h}{g^2 \omega_{m,n}} \widehat{u}_m^* \widehat{u}_n \widehat{U}_{m,n} e^{2k_p z}, \quad (\text{C12})$$

with an error factor  $[1 + O(\alpha, k_p^{-1} h^{-1})]$ . For  $|k_{m,n}|h \gg 1$ , (C12) reduces to (C11).

2.3. Deep water for short wave, shallow water for subharmonic waves  $|k_{m,n}|h \ll 1 \ll O(k_p h)$

In this case the following result can be obtained either from (2.61) similar to the derivation of (A14) or considering  $|k_{m,n}|h \ll 1$  in (C12)

$$\overline{u_L^{(4)}} = \frac{\omega_p}{g} \sum_{m,n} \widehat{U}_{m,n} \widehat{U}_{m,n}^* + \frac{4\omega_p^4 h}{g^3} \sum_{m,n} \widehat{u}_m^* \widehat{u}_n \widehat{U}_{m,n} e^{\frac{2\omega_p^2}{g} z}. \quad (\text{C13})$$

which becomes in time domain

$$\overline{u_L^{(4)}} = \frac{2\omega_p}{g} \overline{\tilde{u}^2} + \frac{8\omega_p^4 h}{g^3} [\overline{u^{(1)}}]^2 \tilde{u}, \quad (\text{C14})$$

with an error factor  $[1 + O(\alpha, k_p^{-1} h^{-1}, k_{m,n}^2 h^2)]$ .

2.4. Intermediate depth for short waves, shallow water for subharmonic waves  $|k_{m,n}|h \ll O(k_p h) = O(1)$

Let  $(k_m h, k_n h) = k_p h[1 + O(\alpha)] = O(1)$  and  $k_{m,n} h \ll O(1)$ , equation (2.61) becomes approximately

$$\begin{aligned} \overline{u_L^{(4)}} &= \sum_{m,n} \frac{\widehat{U}_{m,n} \widehat{U}_{m,n}^*}{2c_g} + \left( \frac{2 \cosh 2k_p(z+h)}{cc_g} + \frac{1}{c^2} \frac{\partial}{\partial \omega} \{ \omega \cosh [2k(z+h)] \} \right. \\ &\quad \left. + \frac{1}{\omega^2} \frac{\partial}{\partial \omega} \{ \omega k^2 \cosh [2k(z+h)] \} \right) \frac{\hat{u}_m^* \hat{u}_n \widehat{U}_{m,n}}{4 \cosh^2 k_p h} \\ &= \sum_{m,n} \frac{\widehat{U}_{m,n} \widehat{U}_{m,n}^*}{2c_g} + \left( \frac{1}{cc_g} [2 + 2k_p(z+h) \tanh [2k_p(z+h)]] + \frac{1}{c^2} \right) \\ &\quad \times \frac{\hat{u}_m^* \hat{u}_n \widehat{U}_{m,n}}{2} \frac{\cosh 2k_p(z+h)}{\cosh^2 k_p h}, \end{aligned} \quad (\text{C15})$$

with an error factor  $[1 + O(k_{m,n}^2 h^2, \alpha)]$  and  $c$  and  $c_g$  take the general expressions as in (A16). Equivalently in time domain (C15) becomes

$$\begin{aligned} \overline{u_L^{(4)}} &= \frac{\tilde{u}^2}{c_g} + \left[ \frac{5}{2} + \frac{k_p h}{\sinh 2k_p h} + 2k_p(z+h) \tanh [2k_p(z+h)] \right] \\ &\quad \times \frac{\cosh 2k_p(z+h)}{\cosh^2 k_p h} \frac{\left[ u^{(1)} \Big|_{z=0} \right]^2 \tilde{u}}{cc_g}. \end{aligned} \quad (\text{C16})$$

For  $k_p h \gg 1$  (C16) reduces to (C14). Integrating (C16) vertically from  $z = -h$  to  $z = 0$  recovers (A22).

## 2.5. Shallow water for both short and subharmonic waves $|k_{m,n}|h \ll O(k_p h) \ll 1$

In this case the result is given by equations (C8)–(C9), which can also be obtained for  $k_p h \ll 1$  in (C16).

## Appendix D. Separation of incident and reflected subharmonic waves

The subharmonic surface elevation was decomposed into the incident ( $\tilde{\eta}^+$ ) and reflected ( $\tilde{\eta}^-$ ) components in the time domain using the weakly nonlinear method proposed by van Dongeren (1997) as per Ruju, Lara & Losada (2012) and Liu *et al.* (2023)

$$\tilde{\eta}^+ = \frac{\sqrt{gh} \tilde{\eta} + \tilde{Q}}{c_g + \sqrt{gh}}, \quad \tilde{\eta}^- = \frac{c_g \tilde{\eta} - \tilde{Q}}{c_g + \sqrt{gh}}, \quad (\text{D1})$$

where  $c_g$  is the group velocity corresponding to the peak frequency;  $\tilde{Q}$  is the low-frequency volume flux per unit obtained by filtering the volume flux  $Q$  through in the infragravity frequency band  $[0, 0.5/T_p]$ . The volume flux  $Q$  was estimated using the surface elevation  $h(x, t)$  and the horizontal velocity  $u(x, z, t)$  measured at a fixed height above the bed as follows.

The volume flux per unit width  $Q$  is defined as

$$Q(t) = \int_{-h}^{\eta} u(z, t) dz, \quad (\text{D2})$$

where we assume the velocity was measured at a fixed height of the probe  $z = z_p$ , which can be expressed as the discrete Fourier series

$$u(z_p, t) = \sum_{f=0}^{1.5f_p} \hat{u}(z_p, f) \exp(-2\pi i f t), \quad (\text{D3})$$

where  $\hat{u}$  denotes the complex amplitude. The upper limit of frequency  $1.5f_p$  is used here to remove the contributions from the flume resonance and superharmonics.

The profile of  $\hat{u}(z, f)$  was then calculated from the single point value of  $\hat{u}(z_p, f)$  using the linear wave theory as  $\hat{u}(z, f) = \hat{u}(z_p, f) \cosh[k(h+z)] / \cosh[k(h+z_p)]$ , with  $k$  being the wavenumber at frequency  $f$ . Therefore, the horizontal velocity in the time domain is given by

$$u(z, t) = \sum_{f=0}^{1.5f_p} \hat{u}(z_p, f) \frac{\cosh[k(h+z)]}{\cosh[k(h+z_p)]} \exp(-2\pi i f t). \quad (\text{D4})$$

Substituting (D4) into (D2) yields

$$Q(t) = \sum_{f=0}^{1.5f_p} \frac{\hat{u}(z_p, f)}{\cosh[k(h+z_p)]} \frac{\sinh[k(h+\eta)]}{k} \exp(-2\pi i f t). \quad (\text{D5})$$

Accurate to the second order in wave steepness, the Taylor expansion  $\sinh[k(h+\eta)] = \sinh kh + k\eta \cosh kh + O(\eta^2)$  is adopted to further reduce (D5) to

$$Q(t) = \sum_{f=0}^{1.5f_p} \frac{\hat{u}(z_p, f) \sinh kh}{k \cosh[k(h+z_p)]} \exp(-2\pi i f t) + \eta \sum_{f=0}^{1.5f_p} \frac{\hat{u}(z_p, f) \cosh kh}{\cosh[k(h+z_p)]} \exp(-2\pi i f t). \quad (\text{D6})$$

The orbital velocity of incident subharmonic wave is obtained by subtracting the reflected component from the total velocity as

$$\tilde{u}^+ = \tilde{u} + \tilde{\eta}^- \sqrt{\frac{g}{h}}. \quad (\text{D7})$$

#### REFERENCES

- DE BAKKER, A.T.M., BRINKKEMPER, J.A., VAN DER STEEN, F., TISSIER, M.F.S. & RUESSINK, B.G. 2016a Cross-shore sand transport by infragravity waves as a function of beach steepness. *J. Geophys. Res. Earth Surf.* **121** (10), 1786–1799.
- DE BAKKER, A.T.M., HERBERS, T.H.C., SMIT, P.B., TISSIER, M.F.S. & RUESSINK, B.G. 2015 Nonlinear infragravity-wave interactions on a gently sloping laboratory beach. *J. Phys. Oceanogr.* **45** (2), 589–605.
- DE BAKKER, A.T.M., TISSIER, M.F.S. & RUESSINK, B.G. 2016b Beach steepness effects on nonlinear infragravity-wave interactions: a numerical study. *J. Geophys. Res. Oceans* **121** (1), 554–570.
- BALDOCK, T.E., ALSINA, J.A., CACERES, I., VICINANZA, D., CONTESTABILE, P., POWER, H. & SANCHEZ-ARCILLA, A. 2011 Large-scale experiments on beach profile evolution and surf and swash zone sediment transport induced by long waves, wave groups and random waves. *Coast. Engng* **58** (2), 214–227.
- BALDOCK, T.E., MANOONVORAVONG, P. & PHAM, K.S. 2010 Sediment transport and beach morphodynamics induced by free long waves, bound long waves and wave groups. *Coast. Engng* **57** (10), 898–916.
- BATTJES, J.A., BAKKENES, H.J., JANSSEN, T.T. & VAN DONGEREN, A.R. 2004 Shoaling of subharmonic gravity waves. *J. Geophys. Res. Oceans* **109** (2), C02009.
- BERTIN, X., DE BAKKER, A., VAN DONGEREN, A., COCO, G., ANDRÉ, G., ARDHUIN, F., BONNETON, P., BOUCHETTE, F., CASTELLE, B., CRAWFORD, W. C., *et al.* 2018 Infragravity waves: from driving mechanisms to impacts. *Earth Sci. Rev.* **177**, 774–799.

- BERTIN, X., MENDES, D., MARTINS, K., FORTUNATO, A.B. & LAVAUD, L. 2019 The closure of a shallow tidal inlet promoted by infragravity waves. *Geophys. Res. Lett.* **46** (12), 6804–6810.
- BERTIN, X. & OLABARRIETA, M. 2016 Relevance of infragravity waves in a wave-dominated inlet. *J. Geophys. Res.: Oceans* **121** (8), 5418–5435.
- BJØRNESTAD, M., BUCKLEY, M., KALISCH, H., STRESSER, M., HORSTMANN, J., FRØYSA, H.G., IGE, O.E., CYSEWSKI, M. & CARRASCO-ALVAREZ, R. 2021 Lagrangian measurements of orbital velocities in the surf zone. *Geophys. Res. Lett.* **48** (21), e2021GL095722.
- BLONDEAUX, P., BROCCINI, M. & VITTORI, G. 2002 Sea waves and mass transport on a sloping beach. *Proc. R. Soc. Lond. A: Math. Phys. Engng Sci.* **458** (2025), 2053–2082.
- BONDEHAGEN, A., KALISCH, H. & ROEBER, V. 2024 Infragravity waves and cross-shore motion – a conceptual study. *Front. Mar. Sci.* **11**, 1374144.
- VAN DEN BREMER, T.S., WHITTAKER, C., CALVERT, R., RABY, A. & TAYLOR, P.H. 2019 Experimental study of particle trajectories below deep-water surface gravity wave groups. *J. Fluid Mech.* **879**, 168–186.
- CALVERT, R., MCALLISTER, M.L., WHITTAKER, C., RABY, A., BORTHWICK, A.G.L. & VAN DEN BREMER, T.S. 2021 A mechanism for the increased wave-induced drift of floating marine litter. *J. Fluid Mech.* **915**, A73.
- CALVERT, R., WHITTAKER, C., RABY, A., TAYLOR, P.H., BORTHWICK, A.G.L. & VAN DEN BREMER, T.S. 2019 Laboratory study of the wave-induced mean flow and set-down in unidirectional surface gravity wave packets on finite water depth. *Phys. Rev. Fluids* **4** (11), 114801.
- CASTELLE, B., SCOTT, T., BRANDER, R.W. & MCCARROLL, R.J. 2016 Rip current types, circulation and hazard. *Earth Sci. Rev.* **163**, 1–21.
- CHEN, Y.-Y., HSU, H.-C. & CHEN, G.-Y. 2010 Lagrangian experiment and solution for irrotational finite-amplitude progressive gravity waves at uniform depth. *Fluid Dyn. Res.* **42** (4), 045511.
- CHEN, Y.-Y., LI, M.-S., HSU, H.-C. & NG, C.-O. 2012 Theoretical and experimental study of particle trajectories for nonlinear water waves propagating on a sloping bottom. *Phil. Trans. R. Soc. A: Math. Phys. Engng Sci.* **370** (1964), 1543–1571.
- CHRISTENSEN, K.H. & TERRILE, E. 2009 Drift and deformation of oil slicks due to surface waves. *J. Fluid Mech.* **620**, 313–332.
- CONTARDO, S., LOWE, R.J., HANSEN, J.E., RIJNSDORP, D.P., DUFOIS, F. & SYMONDS, G. 2021 Free and forced components of shoaling long waves in the absence of short-wave breaking. *J. Phys. Oceanogr.* **51** (5), 1465–1487.
- DAVEY, A. & STEWARTSON, K. 1974 On three-dimensional packets of surface waves.. *Proc. R. Soc. Lond. A, Math. Phys. Sci.* **338** (1613), 101–110.
- DEIGAARD, R., JAKOBSEN, J.B. & FREDSE, J. 1999 Net sediment transport under wave groups and bound long waves. *J. Geophys. Res. Oceans* **104** (C6), 13559–13575.
- DI BENEDETTO, M.H., CLARK, L.K. & PUJARA, N. 2022 Enhanced settling and dispersion of inertial particles in surface waves. *J. Fluid Mech.* **936**, A38.
- DI BENEDETTO, M.H., OUELLETTE, N.T. & KOSEFF, J.R. 2018 Transport of anisotropic particles under waves. *J. Fluid Mech.* **837**, 320–340.
- VAN DONGEREN, A. 1997 Quasi-3D modelling nearshore hydrodynamics. PhD thesis, University of Delaware.
- DRIVDAL, M., BROSTRÖM, G. & CHRISTENSEN, K.H. 2014 Wave-induced mixing and transport of buoyant particles: application to the Statfjord A oil spill. *Ocean Sci.* **10** (6), 977–991.
- FIEDLER, J.W., SMIT, P.B., BRODIE, K.L., MCNINCH, J. & GUZA, R.T. 2019 The offshore boundary condition in surf zone modeling. *Coast. Engng* **143**, 12–20.
- FLORES, R.P., WILLIAMS, M.E. & HORNER-DEVINE, A.R. 2022 River plume modulation by infragravity wave forcing. *Geophys. Res. Lett.* **49** (15), e2021GL097467.
- HENDERSON, S.M. & ALLEN, J.S. 2004 Nearshore sandbar migration predicted by an eddy-diffusive boundary layer model. *J. Geophys. Res. Oceans* **109** (C6), C06024.
- HERBERS, T.H.C. & JANSSEN, T.T. 2016 Lagrangian surface wave motion and Stokes drift fluctuations. *J. Phys. Oceanogr.* **46** (4), 1009–1021.
- HSU, T.-J., ELGAR, S. & GUZA, R.T. 2006 Wave-induced sediment transport and onshore sandbar migration. *Coast. Engng* **53** (10), 817–824.
- ISKANDARANI, M. & LIU, P.L.-F. 1991 Mass transport in two-dimensional water waves. *J. Fluid Mech.* **231**, 395–415.
- JANSSEN, T.T., BATTJES, J.A. & VAN DONGEREN, A.R. 2003 Long waves induced by short-wave groups over a sloping bottom. *J. Geophys. Res. Oceans* **108** (C8), 3252.
- LAXAGUE, N.J., ÖZGÖKMEN, T.M., HAUS, B.K., NOVELLI, G., SHCHERBINA, A., SUTHERLAND, P., GUIGAND, C.M., LUND, B., MEHTA, S., ALDAY, M. & MOLEMAKER, J. 2018 Observations of

- near-surface current shear help describe oceanic oil and plastic transport. *Geophys. Res. Lett.* **45** (1), 245–249.
- LI, M.-S., CHEN, Y.-Y., ZOU, Q. & HSU, H.-C. 2023 Perturbation analysis of nonlinear partial reflected wave on a sloping bottom. *Nonlinear Anal Real World Applics.* **73**, 103885.
- LI, Y., ZHANG, C., ZHAO, S., QI, H., CAI, F. & ZHENG, J. 2024 Equilibrium configurations of sandy-muddy transitional beaches on south China coasts: role of waves in formation of sand-mud transition boundary. *Coast. Engng* **187**, 104401.
- LIAO, Z., LI, S., LIU, Y. & ZOU, Q. 2021 An analytical spectral model for infragravity waves over topography in intermediate and shallow water under nonbreaking conditions. *J. Phys. Oceanogr.* **51** (9), 2749–2765.
- LIAO, Z., ZOU, Q., LIU, Y., CONTARDO, S. & LI, S. 2023 Unified analytical solution for group-induced infragravity waves based on Green's function. *J Fluid Mech.* **967**, A37.
- LIAO, Z., ZOU, Q., VINH, V.D., PAN, Z. & KAISER, M.J. 2024 Seasonal change in fate and transport of plastics from red River to the coast of Vietnam. *Mar. Pollut. Bull.* **208**, 116923.
- LIU, P.L.F. 1989 A note on long waves induced by short-wave groups over a shelf. *J Fluid Mech.* **205**, 163–170.
- LIU, Y., YAO, Y., LIAO, Z., LI, S., ZHANG, C. & ZOU, Q. 2023 Fully nonlinear investigation on energy transfer between long waves and short-wave groups over a reef. *Coast. Engng* **179**, 104240.
- VAN LEEUWEN, P.J. 1992 Low frequency wave generation due to breaking waves. Ph.D. dissertation, Delft University of Technology, Delft, Netherlands.
- LONGUET-HIGGINS, M.S. 1953 Mass transport in water waves. *Phil. Trans. R. Soc. Lond. A, Math. Phys. Sci.* **245** (903), 535–581.
- LONGUET-HIGGINS, M.S. 1960 Mass transport in the boundary layer at a free oscillating surface. *J Fluid Mech.* **8** (2), 293–306.
- LONGUET-HIGGINS, M.S. 1969 On the transport of mass by time-varying ocean currents. *Deep Sea Res. Oceanogr. Abstract* **16** (5), 431–447.
- LONGUET-HIGGINS, M.S. & STEWART, R.W. 1962 Radiation stress and mass transport in gravity waves, with application to surf beats. *J Fluid Mech.* **13** (4), 481–504.
- MCALLISTER, M.L. & VAN DEN BREMER, T.S. 2019 Lagrangian measurement of steep directionally spread ocean waves: second-order motion of a wave-following measurement buoy. *J. Phys. Oceanogr.* **49** (12), 3087–3108.
- MEI, C.C., MICHAEL, S., YUE, D.K.-P. & MEI, C.C. 2005 Theory and applications of ocean surface waves. MENDES, D., FORTUNATO, A.B., BERTIN, X., MARTINS, K., LAVAUD, L., NOBRE SILVA, A., PIRES-SILVA, A.A., COULOMBIER, T. & PINTO, J.P. 2020 Importance of infragravity waves in a wave-dominated inlet under storm conditions. *Cont. Shelf Res.* **192**, 104026.
- MILES, J. 2013 Wave shape effects on sediment transport. *J. Coast. Res.* **165**, 1803–1808.
- MONISMITH, S.G., COWEN, E.A., NEPF, H.M., MAGNAUDET, J. & THAIS, L. 2007 Laboratory observations of mean flows under surface gravity waves. *J Fluid Mech.* **573**, 131–147.
- MUNK, W.H. 1949 Surf beats. *EOS, Trans. Am. Geophys. Union* **30** (6), 849–854.
- NG, C. 2004a Mass transport in gravity waves revisited. *J. Geophys. Res. Oceans* **109** (C4), C04012.
- NG, C.-O. 2004b Mass transport and set-ups due to partial standing surface waves in a two-layer viscous system. *J Fluid Mech.* **520**, 297–325.
- NIELSEN, P. 2006 Sheet flow sediment transport under waves with acceleration skewness and boundary layer streaming. *Coast. Engng* **53** (9), 749–758.
- NORHEIM, C.A., HERBERS, T.H.C. & ELGAR, S. 1998 Nonlinear evolution of surface wave spectra on a beach. *J. Phys. Oceanogr.* **28** (7), 1534–1551.
- NÚÑEZ, P., ROMANO, A., GARCÍA-ALBA, J., BESIO, G. & MEDINA, R. 2023 Wave-induced cross-shore distribution of different densities, shapes, and sizes of plastic debris in coastal environments: a laboratory experiment. *Mar. Pollut. Bull.* **187**, 114561.
- RIJNSDORP, D.P., RUESSINK, G. & ZIJLEMA, M. 2015 Infragravity-wave dynamics in a barred coastal region, a numerical study. *J. Geophys. Res. Oceans* **120** (6), 4068–4089.
- RIJNSDORP, D.P., SMIT, P. & ZIJLEMA, M. 2014 Non-hydrostatic modeling of infragravity waves under laboratory conditions. *Coast. Engng* **85**, 30–42.
- RUESSINK, B.G., MICHALLET, H., ABREU, T., SANCHE, F., VAN DER A, D.A., VAN DER WERF, J.J. & SILVA, P.A. 2011 Observations of velocities, sand concentrations, and fluxes under velocity-asymmetric oscillatory flows. *J. Geophys. Res. Oceans* **116** (C3), 3004.
- RUESSINK, B.G., MICHALLET, H., BONNETON, P., MOUAZE, D., LARA, J. & 2013 Globex: wave dynamics on a gently sloping laboratory beach. In *7th International Conference on Coastal Dynamics*, pp. 1351–1362. ASME.
- RUJU, A., LARA, J.L. & LOSADA, I.J. 2012 Radiation stress and low-frequency energy balance within the surf zone: a numerical approach. *Coast. Engng* **68**, 44–55.

- RUSSELL, P.E. 1993 Mechanisms for beach erosion during storms. *Cont. Shelf Res.* **13** (11), 1243–1265.
- RUSSELL, R.C.H. & OSORIO, J.D.C. 1957 An experimental investigation of drift profiles in a closed channel. *Coast. Engng Proc.* **6** (6), 10.
- SCHÄFFER, H.A. 1993 Infragravity waves induced by short-wave groups. *J Fluid Mech.* **247** (2), 551–588.
- VAN SEBILLE, E., ALIANI, S., LAW, K.L., MAXIMENKO, N., ALSINA, J.M., BAGAEV, A., BERGMANN, M., CHAPRON, B., CHUBARENKO, I., CÓZAR, A., *et al.* 2020 The physical oceanography of the transport of floating marine debris. *Environ. Res. Lett.* **15** (2), 023003.
- SHEPARD, D. 1968 A two-dimensional interpolation function for irregularly-spaced data. In *Proceedings of the 1968 23rd ACM National Conference*, pp. 517–524. ACM.
- SHEREMET, A., GUZA, R.T., ELGAR, S. & HERBERS, T.H.C. 2002 Observations of nearshore infragravity waves: seaward and shoreward propagating components. *J. Geophys. Res. Oceans* **107** (C8), 10-1.
- SMIT, P.B., JANSSEN, T.T., HOLTHUIJSEN, L. & SMITH, J.J. 2014 Non-hydrostatic modeling of surf zone wave dynamics. *Coast. Engng* **83**, 36–48.
- STOKES, G.G. 1847 On the theory of oscillatory waves. *Trans. Cam. Philos. Soc.* **8**, 441–455.
- SYMONDS, G., HUNTLEY, D.A. & BOWEN, A.J. 1982 Two-dimensional surf beat: long wave generation by a time-varying breakpoint. *J. Geophys. Res.* **87** (C1), 492–498.
- VAN THIEL DE VRIES, J.S.M., VAN GENT, M.R.A., WALSTRA, D.J.R. & RENIERS, A.J.H.M. 2008 Analysis of dune erosion processes in large-scale flume experiments. *Coast. Engng* **55** (12), 1028–1040.
- TUCKER, M.J. 1950 Surf beats: sea waves of 1 to 5 min. period. *Proc. R. Soc. Lond. A Math. Phys. Sci.* **202** (1071), 565–573.
- URSELL, F. 1953 The long-wave paradox in the theory of gravity waves. *Math. Proc. Cam. Phil. Soc.* **49** (4), 685–694.
- VITTORI, G. & BLONDEAUX, P. 1996 Mass transport under sea waves propagating over a rippled bed. *J Fluid Mech.* **314**, 247–265.
- WILLIAMS, M.E. & STACEY, M.T. 2016 Tidally discontinuous ocean forcing in bar-built estuaries: the interaction of tides, infragravity motions, and frictional control. *J. Geophys. Res.: Oceans* **121** (1), 571–585.
- YU, X., HSU, T.J. & HANES, D.M. 2010 Sediment transport under wave groups: relative importance between nonlinear wavelike and nonlinear boundary layer streaming. *J. Geophys. Res. Oceans* **115** (2), C02013.
- ZIJLEMA, M., STELLING, G. & SMIT, P. 2011 SWASH: an operational public domain code for simulating wave fields and rapidly varied flows in coastal waters. *Coast. Engng* **58** (10), 992–1012.
- ZOU, Q. 2002 An analytical model of wave bottom boundary layers incorporating turbulent relaxation and diffusion effects. *J. Phys. Oceanogr.* **32** (9), 2441–2456.
- ZOU, Q. 2011 Generation, transformation, and scattering of long waves induced by a short-wave group over finite topography. *J. Phys. Oceanogr.* **41** (10), 1842–1859.
- ZOU, Q., BOWEN, A.J. & HAY, A.E. 2006 Vertical distribution of wave shear stress in variable water depth: theory and field observations. *J. Geophys. Res. Oceans* **111** (9), C09032.
- ZOU, Q. & HAY, A.E. 2003 The vertical structure of the wave bottom boundary layer over a sloping bed: theory and field measurements. *J. Phys. Oceanogr.* **33** (7), 1380–1400.